Brune

THE CHARACTER OF HIGH-FREQUENCY STRONG GROUND MOTION

Thomas C. Hanks[1] and Robin K. McGuire[2]

Abstract

Analysis of more than 300 horizontal components of ground accelerations written by the San Fernando earthquake, eight other moderate-to-large California earthquakes, and seven Oroville aftershocks reveal that these acceleration time histories are, to a very good approximation, band-limited, white, Gaussian noise within the S-wave arrival window; the band limitation is defined by the spectral corner frequency f_o and f_{max}, the highest frequency passed by the accelerograph or the Earth's attenuation operator, and the S-wave arrival window is $(0 \leq t-R/\beta \leq T_d)$, where R is distance, β is shear-wave velocity and T_d is the faulting duration. An examination of the root-mean-square acceleration (a_{rms}) characteristics of these records for $0 \leq t - R/\beta \leq T_d$ in terms of the relation

$$a_{rms} = 0.85 \frac{(2\pi)^2}{106} \frac{\Delta\sigma}{\rho R} \sqrt{\frac{f_{max}}{f_o}}$$

where $\Delta\sigma$ is the earthquake stress drop, yields the surprising result that all 16 earthquakes have stress drops, as determined by record values of a_{rms}, very nearly equal to 100 bars (± a factor of 2). The source dependence of

---

1 U.S. Geological Survey. 345 Middlefield Road, Menlo Park, California 94025

2 Ertec, Inc., 14142 W. 20th Avenue, Golden, Colorado 80401

a_{rms} thus depends solely on the parameter $1/\sqrt{f_o}$, which increases only as the one-sixth power of seismic moment for constant stress drop earthquakes. Put another way, model and record a_{rms} are in agreement within a factor of 2 approximately 85 percent of the time for $\Delta\sigma$ = 100 bars and knowledge of $1/\sqrt{f_o}$.

On the basis that acceleration time histories are finite-duration, band-limited, white, Gaussian noise, for any of which a_{rms} is fixed by $\Delta\sigma$ = 100 bars and $1/\sqrt{f_o}$, we can estimate the peak accelerations (a_{max}) for all of these records with considerable accuracy (50 percent or less). The relation is

$$a_{max} = a_{rms}\sqrt{2\ln\left(\frac{2f_{max}}{f_o}\right)} \quad ,$$

where a_{rms} is defined above. With less accuracy, this relation fits the peak acceleration set of Hanks and Johnson (1976) as well, again with $\Delta\sigma$ = 100 bars. At a fixed, close distance, we determine the magnitude dependence of a_{max} to be $\log a_{max} \sim 0.30\,M$ for $4 \leq M = M_L \leq 6\ 1/2$, remarkably close to that recently determined empirically by Joyner et al (1981) for $5.0 \leq M \leq 7.7$, their coefficient on M (moment magnitude) being 0.28 ± 0.04. In the model presented here, the magnitude-dependence of peak acceleration is a function of faulting duration alone; larger earthquakes have larger peak accelerations because they last longer, not because they are intrinsically more powerful.

These well-behaved characteristics of high-frequency strong ground motion also suggest that the stress differences which develop in the course of crustal faulting are comparably well-behaved, both in the average stress release across the characteristic source dimension and in the spectral composition and distribution of stress differences that develop across smaller dimensions.

INTRODUCTION

Earthquake ground motion at periods short compared to the faulting duration has attracted the attention of seismologists and engineers alike in recent years, principally through the realization that existing characterizations of high-frequency strong ground motion in terms of causative faulting processes or in terms of potential for structural damage are at best rudimentary. There is considerable seismological interest in how high-frequency ground motion data might be used to infer the character of quasi-static and dynamic stress differences which are associated with crustal faulting and how such inhomogeneities might condition the cause and effect of crustal earthquakes. In a related vein, it is still a matter of vigorous debate whether or not $M \geq 6$ crustal earthquakes are organized and coherent enough in the real Earth to materially affect high-frequency amplitudes (for example, peak acceleration) in a limited azimuthal range via source directivity effects (e.g. Brune and Blume, 1981). Finally, there is has been much recent interest in magnitude saturation and how this phenomenom might work for peak acceleration at some fixed, close distance -- or might not work.

From an engineering perspective, it has long been appreciated that peak acceleration does not correlate particularly well with all types of structural damage (Blume, 1979). While this might be expected from recent studies indicating that peak acceleration depends only weakly on magnitude at close distances (e.g. Hanks and Johnson, 1976; Joyner et al, 1981), it surely must be of concern to both engineers and seismologists that the most widely used measure of high-frequency strong ground motion over the past five decades is not a particularly good measure of real or potential structural damage. But

if peak acceleration isn't, what is? While considerable attention has been paid by the engineering community to the notion of "effective peak acceleration," it is yet without a "precise definition in physical terms" (Applied Technology Council, 1978, p. 298). Moreover, it seems almost certain that the duration of high-frequency strong ground motion at some fixed level of amplitudes will play an important role in producing structural damage (and that any definition of effective peak acceleration will have to incorporate duration effects), but this problem has received very little quantitative attention.

Although we shall be more precise about the matter shortly, by "high-frequency strong ground motion" we mean in this study ground acceleration in the frequency band from ≈ 1 Hz up to the highest frequency (f_{max}) passed by the Earth's attenuation operator or the instrumental recording system, with amplitudes sufficiently large to be of engineering concern. Thus, as a formal matter of frequency band, the concept of high-frequency strong ground motion as investigated here is fully complementary to that of long-period strong-ground motion (e.g. Hanks, 1975; 1979b). This distinction between high-frequency and long-period strong ground motion runs more deeply, however, since there is an important deterministic character of long-period strong ground motion, easily discernible in both amplitude and phase, that is generally absent in high-frequency strong ground motion.

Ground motion observations and theoretical modeling are in accord that at source-station distances greater than two source depths, strong ground motion at periods $\gtrsim$ 1 sec will generally be dominated by surface waves, especially in sedimentary basins where near-surface impedance contrasts dramatically enhance the surface wave contributions (Hanks, 1975, 1976; Heaton and Helmberger,

1977, 1978; Swanger and Boore, 1978a,b; Kudo, 1978). Indeed, when layered half-space models are a reasonable approximation to the Earth structure for the source-station pair of interest, the observed long-period strong ground motion can be synthesized with striking accuracy (e.g., Heaton and Helmberger, 1977; Swanger and Boore, 1978a).

At frequencies of 2 Hz and greater, however, the character of strong ground motion is considerably more complicated, principally because of the loss of phase coherence across even very small station separations (Figure 1). At these frequencies, $M \gtrsim 6$ earthquakes can be almost arbitrarily complicated, and it is not to be expected that wave propagation effects at such frequencies will be much simpler, given any heterogeneity at all in crustal structure. In view of the complicated phase interference in Figure 1, it is safe to say that it will be impossible to deterministically synthesize high-frequency strong ground motion in the time domain (that is, acceleration time histories) except under rather unusual circumstances which, in general, will involve small station-spacing ($\lesssim 2$ km), small ($M \lesssim 5$) simple earthquakes at close ($R \lesssim 10$ km) distances, and uncomplicated geology. Evidently, a realistic characterization of high-frequency strong ground motion will require one or more stochastic parameters that can account for phase incoherence.

In the context of these matters, we here explore further the efficacy of the root-mean-square acceleration (a_{rms})/faulting duration (T_d) pair as a measure of high-frequency strong ground motion for seismologic and engineering purposes, using the recent studies of Hanks (1979a) and McGuire and Hanks (1980) as the point of departure. Since a_{rms} can only be defined for some interval or "duration" of ground motion and since observed ground motion durations seem plainly to be a function of period and distance, some attention is paid to this matter in the next (second) section, wherein the model

a_{rms} estimates of Hanks (1979a) and McGuire and Hanks (1980) are briefly recapitulated. In the third section, the model estimates are exercised against record values for a set of eight moderate-to-large California earthquakes and seven aftershocks of the Oroville, California, earthquake (Aug 1, 1975; M_L = 5.7). These comparisons, together with those of McGuire and Hanks (1980) for the San Fernando earthquake (Feb. 9, 1971; M_L=6.4), produce the surprising result that, as measured by their high-frequency excitation, these earthquakes all seem to have stress drops very close to 100 bars (variations of about a factor of 2), despite the variations in their stress drops as determined by conventional means of about a factor of 50.

In the fourth section a comparison of the peak accelerations to the record a_{rms} values reveals, also surprisingly, that peak acceleration is as stable a measure of high-frequency strong ground motion as a_{rms}. Assuming that far-field, ground accelerations are finite-duration, band-limited, white, Gaussian noise, we are able to estimate the peak acceleration data from the San Fernando earthquake records (McGuire and Hanks, 1980), from the Oroville aftershocks and other California earthquakes studied here, and from the peak acceleration set of Hanks and Johnson (1976) -- altogether almost 400 values -- with reasonable accuracy. In the fifth section, we verify directly with frequency-of-occurrence counts that acceleration amplitudes within the time interval T_d beginning with the direct shear arrival distribute in a nearly Gaussian manner. Finally, we discuss the significant potential the results of this study hold for estimating high-frequency strong ground motion for engineering purposes and for inferring the nature of stress differences that arise in the course of crustal faulting.

THE MODEL ESTIMATE OF a_{rms}

Hanks (1979a) and McGuire and Hanks (1980) have demonstrated how an operation of Parseval's theorem on the Brune (1970, 1971) source model may be used to estimate a_{rms} for far-field shear waves in the presence of anelastic attenuation. The estimate may be written

$$a_{rms} = 2R_{\theta\phi} \frac{(2\pi)^2}{106} \frac{\Delta\sigma}{\rho R^{3/2}} \sqrt{\frac{Q\beta}{\pi f_o}} \qquad (1)$$

or

$$a_{rms} = 2R_{\theta\phi} \frac{(2\pi)^2}{106} \frac{\Delta\sigma}{\rho R} \sqrt{\frac{f_{max}}{f_o}}, \quad f_{max} = \frac{Q\beta}{\pi R} \qquad (2)$$

when the anelastic attenuation of spectral amplitudes is of the form $e^{-\pi fR/Q\beta}$; alternatively, f_{max} may be set equal to the natural frequency of the accelerograph if this is the controlling factor. In these relations, R is hypocentral distance, Q^{-1} is specific attenuation, β is shear-wave velocity, ρ is density, f_o is the spectral corner frequency of the far-field shear radiation, and $\Delta\sigma$ is the earthquake stress drop. $R_{\theta\phi}$ is the radiation pattern in the coordinates of the instrumental axes. In Hanks (1979a) and McGuire and Hanks (1980), the rms-value for shear excitation $R_{\theta\phi} = 0.6$ was used, together with the assumption that the energy was equally partitioned into two horizontal components. With these assumptions, the factor of $2R_{\theta\phi}$ becomes 0.85, the leading factor of 2 accounting for free-surface amplification.

It is implicit in these a_{rms} estimates that, in the absence of anelastic attenuation, the far-field acceleration would be white for $f \geq f_o$ (and in the presence of anelastic attenuation approximately white in the band

$f_0 \leq f \leq f_{max}$). This corresponds to the $\omega^{-\gamma}$, $\gamma = 2$, model of far-field shear-displacement spectral amplitudes. Hanks (1979a) has argued that the $\gamma = 2$ model is the one generally but certainly not always applicable to crustal earthquakes, but, in fact, very little is known in detail about the form and variability of high-frequency source excitation, with the exception of the San Fernando earthquake (Berrill, 1975). Interestingly enough, the construction of synthetic accelerograms on the basis of finite-duration, band-limited, white noise in acceleration, an engineering approach to strong ground motion for more than 30 years (e.g., Housner, 1947, and numerous more recent studies), is consistent with the ω^{-2} model in the presence of anelastic attenuation. As it turns out, the results of this study provide substantial additional support for the $\gamma = 2$ model of high-frequency excitation, although there remains a possibility of a trade-off between it and the earthquake stress drop, a matter to which we will return.

A second implicit matter concerns the duration of motion over which the model or record estimates of a_{rms} are to be constructed. For the model estimates of (1) or (2), it is clearly the faulting duration (T_d) which is of interest. Observational experience (e.g., Fletcher et al., 1980) as well as theoretical expectations (e.g., Brune, 1970; Hanks, 1979a) suggest that T_d is closely allied with reciprocal f_0, so long as estimates of f_0 unbiased by wave propagation and/or directivity effects are available. As in Hanks (1979a) and McGuire and Hanks (1980), we use here

$$T_d = (f_0)^{-1} \qquad (3)$$

in conjunction with (1) and (2).

The faulting duration, however, is not the same as the ground motion duration of an actual record. Quantifying ground motion duration is a tricky business (McGuire and Barnhard, 1979), principally because ground motion duration is, in general, an increasing function of period and distance (Figure 2). When this is the case, it is almost always the result of waveguide effects, such as travelling surface waves, that result in delayed arrivals. Figure 2 illustrates how this works, in the context of how peak ground-motion values can be contaminated when duration effects are not accounted for. The left-hand side of Figure 2, from top to bottom, plots peak displacement, velocity, and acceleration along a profile of stations extending to the southeast of the San Fernando earthquake (Profile 1 of Hanks, 1975). The curves of the form R^{-n} are not meant to fit the data in any quantitative sense, only to demonstrate that peak displacements decay less rapidly than peak velocities which in turn decay less rapidly than peak accelerations. This is the expected result; the surprising result, in view of what has been said earlier about the progressive loss of coherence in passing to higher frequencies, is that the peak accelerations decay with no more and seemingly less scatter than do the velocities and displacements. The reason for this is indicated on the right side of Figure 2 where the arrival time of the peak amplitude relative to S! (a high-frequency direct shear arrival, Hanks, 1975) is plotted against distance. The peak accelerations at all distances ($32 \leq R \leq 139$ km) arrive in the 10-second body (S)-wave arrival window, but for the peak velocities and displacements this is only true at the closest distances ($R \leq 43$ km). Thus, the latter data sets mix body-wave and surface-wave amplitudes, leading to additional scatter. Since the ordinate values on the right-hand side of Figure 2 are a minimum estimate of ground

motion duration, one may infer that, in general, ground-motion duration increases with period and distance.

Nevertheless, the faulting duration is, except in very unusual circumstances involving strong directivity effects, a lower bound to the ground motion duration. Moreover, our experience and Figure 2 suggest that the ground motion duration converges to the faulting duration at high enough frequencies (specifically those of interest in this study) and/or at close enough distances. Since the principal contributions to the a_{rms} values determined observationally in this study come from high-frequency ($f \gtrsim 2$ Hz) acceleration amplitudes, it is our point of view that the faulting duration is a reasonable estimate of the duration of the high-frequency ground motion of interest. In any event, nominal variations in duration estimates (±50 percent) have little effect on the resulting a_{rms}, at least for the San Fernando earthqauke (McCann, 1980).

Finally, equations (1) and (2) are expressions for the far-field radiation, specifically that the incoming radiation arrives as bodily shear waves. The "far-field" assumption in fact involves two conditions, one that the observation distance R be much greater than the maximum wavelengths of interest in the radiated field and the other that R be much greater than the dimension of the source of the radiation. Because a_{rms}, both theoretically and observationally, depends so heavily on frequencies in excess of 5 Hz, the first condition is not much of a problem. Neither is the second, <u>if</u> we can assume that, for the acceleration amplitudes of interest here, we can simply add up the effects of many small, localized, and isolated bursts to obtain the net effect over T_d, equivalently the much larger dimension of the final faulted surface. This, too, seems, reasonable if the acceleration time histories are so white, random, and Gaussian as we find them to be. Even so,

we are not verifying the far-field assumption for the analysis presented herein; we are simply making it. One problem remains, that for a site close to a major earthquake, for which R can vary greatly from the closest approach (say, 10 km or less) to the nethermost faulting location (perhaps 50 km or more). In the framework here, this would necessitate "partitioning" such an earthquake into ≈ 10 km segments and adding up the effects for appropriate distance and temporal delay. This is easy enough to do in principle, but it does involve some additional assumptions; in the absence of firm observational constraints on this problem, we do not here address it in any quantitative way.

Thus, we are investigating, both observationally and theoretically, a_{rms} as a measure of high-frequency strong ground motion across a time window given by the faulting duration and beginning with the direct shear arrival. It shall be left as implicit that the surface wave contributions (that is, the long-period strong ground motion) may be constructed separately so to synthesize ground motion across the entire frequency band of engineering interest. This shall result in a narrow frequency band that will, in effect, be counted twice, but it involves small enough frequencies that its contribution to a_{rms} is safely negligible.

COMPARISON OF MODEL TO RECORD ESTIMATES OF a_{rms}

To compare the model a_{rms} estimates with those obtained from the recorded accelerograms, we need to know two parameters of the causative earthquake ($\Delta\sigma$, f_0), three properties of the medium (ρ, β, and Q), hypocentral distance R, and the time window for the record estimate ($0 \leq t - R/\beta \leq T_d$). For ρ, β, and Q, we assume conventional values of

2.7 gm/cm^3, 3.2 km/sec and 300, respectively, unless otherwise specified. The first set of data analyzed in this section is a group of eight California earthquakes, each contributing a small number of significant records to the series "Strong Motion Earthquake Accelerograms" prepared by the Earthquake Engineering Research Laboratory of the California Institute of Technology. The source parameters of these earthquakes, mostly determined without reference to the strong-motion accelerograms analyzed here, are culled or estimated from published studies; altogether we investigate 25 strong-motion accelerograms in this set (50 horizontal components). The second set of observations are for seven Oroville aftershocks, each writing about ten strong-motion accelerograms at R ≈ 10 km.

A. The Larger California Earthquakes

Table 1 lists the source parameters of these earthquakes, references to those estimates, and the strong motion accelerograms of these earthquakes analyzed in this study, identified according to the format of the series "Strong Motion Earthquake Accelerograms". These event-record combinations span a considerable range in source strength ($5.3 \leq M \leq 7.7$; $1 \times 10^{24} \leq M_o \leq 2 \times 10^{27}$ dyne-cm), in hypocentral distance ($12 < R \leq 130$ km) and in stress drop ($6 \leq \Delta\sigma \leq 140$ bars). While M_o for these earthquakes are probably accurate to ± 50 percent, with the possible exception of the Wheeler Ridge earthquake for which only one, single-station estimate is available, the $\Delta\sigma$ estimates are less precise; they are no more than "consensus" values through the referenced studies. For the Borrego Mountain earthquake, we have not attempted such a consensus estimate and investigate two end-member models.

Otherwise, we estimate that the $\Delta\sigma$ estimates are accurate to a factor of 3 or so and the $T_d = f_o^{-1}$ estimates are accurate to ± 50 percent, again with the possible exception of the Wheeler Ridge earthquake.

Figure 3 compares the ratio of record/model a_{rms} estimates to the earthquake stress drops (Table 1). Here, the "agreement" between model and record is perhaps best described as bad; for example, the record estimate for the Wheeler Ridge earthquake is almost 20 times larger than for the model estimate. Figure 3 does suggest, however, that the magnitude of the mismatch is a strong function of $(\Delta\sigma)^{-1}$, with an intercept at $\Delta\sigma \simeq 100$ bars for a record/model a_{rms} ratio of 1. In Figure 4, then, we blindly recompute the model values on the basis of the given M_o and $\Delta\sigma = 100$ bars. This necessitates small changes in f_o (e.g. through the use of equation (9) below), and the record estimates are recomputed on the basis of the new T_d's (although the record estimates change only slightly). With a full range scatter of about a factor of 6 and thus a standard deviation of $\sim \sqrt[4]{6}$, the model and record estimates are linearly related; Figure 4 suggests that a stress drop slightly greater than 100 bars would "fit" the data slightly better. But why are the published estimates of $\Delta\sigma$ seemingly low, very much so in some cases? And why do these events, insofar as their high-frequency excitation is concerned, seem to exhibit the same stress drop of about 100 bars, ± a factor of ~ 2? Temporarily, we set these issues aside to present similar comparisons for the seven Oroville aftershocks.

B. The Oroville Aftershocks

To analyze the Oroville aftershocks, we take the inverse approach to that described previously, since otherwise we would be forced to use stress drops obtained from the same records we wish to investigate with respect to a_{rms}. That is, for each component of motion for each aftershock we estimate $\Delta\sigma$ by inverting equation (2). In abbreviated form the result is

$$\Delta\sigma = .19R\sqrt{f_o}\, a_{rms} \qquad (4)$$

where we have set $\rho = 3.0$ gm/cm^3, $\beta = 3.6$ km/sec (Seekins et al, 1978) and $2R_{\theta\phi} = 0.85$, an assumption we discuss in more detail below; and where $\Delta\sigma$ is in bars, R is in km, and a_{rms} (cm/sec^2) is the record estimate determined for a duration of acceleration beginning with the S wave and lasting for $\sim (f_o)^{-1}$. Geometric means of the spectrally determined f_o's for each aftershock (Fletcher et al, 1981) are given in Table 2; f_{max} has been set equal to 25 Hz, the nominal natural frequency of the SMA-1 recording devices.

Table 2 is constructed in the same way as Table 1 of Seekins and Hanks (1978), which gives peak accelerations for all of the source-station pairs in Table 2. For each source-station pair for which a usable record exists (a positively identified record triggering prior to the S wave), Table 2 gives two values of $\Delta\sigma$, one for each horizontal component of motion. The principal result to be extracted from Table 2 is identical to the one we obtained in the last section: in order to square record and model estimates, stress drops very nearly equal to 100 bars are required. The last column of Table 2 gives arithmetic and logarithmic averages of the stress drop estimates for each

earthquake, excluding DJR and DWR for which strong site resonances exist (Seekins and Hanks, 1978).

Despite the nearly monochromatic (at ≈ 20 Hz) visual appearance of the DWR accelerograms, the $\Delta\sigma$'s obtained from a_{rms} at DWR are generally in agreement with those from other stations. This is certainly not the case at DJR, where the $\Delta\sigma$'s so obtained are considerably greater (by factors of 2 to 4) than the average value. Since estimates from all other stations are much more tightly distributed about the means, something clearly anomalous is occurring at DJR. At first glance, this would appear to be the strong site resonance at ≈ 6 Hz that always affects the DJR accelerograms, but similar difficulties with velocity, radiated energy, and displacements have also been encountered for the DJR records (e.g. Fletcher et al, 1980; J. L. Boatwright, personal communication). In view of these unusual ground motion characteristics at DJR for the aftershocks, it is probably not coincidental that very substantial damage was done to the wood-frame residence at this site at the time of the mainshock.

Five of the seven aftershocks have average stress drops between 87 and 101 bars (arithmetic averaging), very constant stress drops indeed by conventional seismological standards (e.g. Hanks, 1977). The other two have average stress drops of about twice as much. In all cases, the standard deviations are only fractions of the average value. Excluding DWR and DJR, Table 2 gives 104 $\Delta\sigma$ estimates, of which only 6 are less than 50 bars and only 10 are greater than 200 bars; all but one of the latter group are associated with the two higher stress drop events 0350 and 2234. The significance of this result is two-fold. First, using $\Delta\sigma$ = 100 bars, one can estimate a_{rms} that will agree with the observations within a factor of 2 most of the time (~ 85 percent).

Second, a_{rms} is a remarkably stable measure of high-frequency strong ground motion; the $\Delta\sigma$ estimates in Table 2 are a fairly transparent image of a_{rms}, since f_o is the same for any aftershock (and does not vary much across the set) and since R varies only between 10 and 15 km for most source-station pairs.

Moreover, the record a_{rms} estimates, as reflected by the $\Delta\sigma$ estimates, depend only weakly, if at all, on the shear-wave radiation pattern. Table 3 compares, for the 0231 aftershock, the stress drop estimates normalized by the average value $\overline{\Delta\sigma}$ = 101 bar for each component of motion to the radiation pattern coefficient normalized by $\langle R_{\theta\phi} \rangle$ = 0.6 for the same component of motion. The coefficient 1.76 simply centers the $R_{\theta\phi}/\langle R_{\theta\phi} \rangle$ distribution at unity for easier comparison with the $\Delta\sigma/\overline{\Delta\sigma}$ distribution. According to equations (1) and (2), $\Delta\sigma/\overline{\Delta\sigma}$ should have an inverse relationship to $R_{\theta\phi}/\langle R_{\theta\phi} \rangle$, since for all $\Delta\sigma$ estimates in Tables 2 and 3 we have used $\langle R_{\theta\phi} \rangle$ = 0.6. No such correlation exists in Table 3. Moreover, the form of the two distributions is grossly different: while the $\Delta\sigma/\overline{\Delta\sigma}$ estimates vary over a total range of a factor of 2, $R_{\theta\phi}/\langle R_{\theta\phi} \rangle$ varies over 2 orders of magnitude. Evidently, the excitation of high-frequency motion is far more isotropic than double-couple point source models allow -- or that scattering mechanisms along the propagation path give this appearance. If this is indeed a source effect, as we tentatively conclude three sections hence, it can only mean that the high-frequency radiation arises from faulting processes far more complicated than a point-source representation. Neither does a_{rms} appear to be closely related to site geology, with the exception of DJR, although the peak acceleration data showed a gross distinction between sedimentary and hard-rock sites (Seekins and Hanks, 1978).

C. Discussion

It is a surprising result that the observed high-frequency ground motion of these 15 earthquakes suggests, according to (1), (2), and (4), that all have stress drops very nearly equal to 100 bars. Our study of the San Fernando earthquake (McGuire and Hanks, 1980) produced the same result, although we did not appreciate it as such at that time: a stress drop of 100 bars would have fit the data better (and in an absolute sense very well) than the 50 bars we actually used (Figure 4 of McGuire and Hanks, 1980). Formally at least, all of these stress drops are the average static stress drops determined from the Brune (1970, 1971) scaling, although they have been estimated differently here from what is conventionally done (e.g. Hanks and Wyss, 1972; Thatcher and Hanks, 1973; Tucker and Brune, 1973). The enigma is that, in a set of 16 earthquake stress drops with such a diverse range in magnitude and tectonic setting, there is no reason to expect they would be so nearly the same ($10^{2 \pm 0.3}$ bars). While the constancy of earthquake stress drops has been a long-recognized seismological phenomenom, it has ordinarily been in the context of estimates distributing over two orders of magnitude (e.g. Hanks, 1977), not ± a factor of 2. More specifically, our results for stress drops differ from those published for the eight earthquakes in Table 1 and for the San Fernando earthquake, often by a considerable margin. When it exists, however, the problem is always that the published stress drops are lower than the ones determined here. Certainly it is possible to underestimate stress drops; whether the source dimension is estimated spectrally or from aftershock dimensions, it is far more likely that a value too large will be obtained than one too small, thus leading to underestimated stress drops.

Irrespective, however, of the biasing problems that might affect this set of data, why is it that all of these earthquakes, given their record a_{rms} values, seem to have such nearly coincident stress drops of 100 bars, as determined from (1), (2) and (4), no matter what the conventionally determined value? We do not know the answer to this question, but we suspect that some tradeoff might exist between the stress drop as estimated in the published studies and the high-frequency spectral decay rate (implicit and fixed at $\gamma = 2$ in (1) and (2)). That is, if $\Delta\sigma$ is less than 100 bars and γ is less than 2 or if $\Delta\sigma$ is greater than 100 bars and γ is greater than 2, it is possible, at least in principle, that the same a_{rms} would result as for $\Delta\sigma = 100$ bars and $\gamma = 2$.

Given the available observations, it is premature to press this possible connection between $\Delta\sigma$ and γ too far, but it is potentially of some seismological significance since $\Delta\sigma$ and γ are generally considered to be independent quantities. Nevertheless, there has been, recently, considerable interest in what relations might exist between frequency-magnitude statistics (b-values), $\Delta\sigma$, and γ (e.g., Hanks, 1979a; Andrews, 1980), and the results of this section provide at least some justification for further consideration of these issues. From the point of view of estimating a_{rms} as a measure of strong ground motion for engineering purposes, however, these matters make no real difference. The observed a_{rms} values for the 176 horizontal components records considered in this study and the 160 horizontal compared considered in the study of the San Fernando earthquake (McGuire and Hanks, 1980) are estimated with remarkable accuracy using $\Delta\sigma = 100$ bars and (1) and (2); most of the observations, with the consistent exception of those at DJR, are within a factor of 2 of this estimate.

PEAK ACCELERATIONS

The value of peak acceleration as a measure of strong ground motion for engineering purposes has come under close scrutiny in recent years, despite the central role it has played in these matters since the first strong motion accelerograms were written almost 50 years ago. In the first place, there is considerable question concerning the reliability of peak acceleration as a measure of damage potential (e.g., Blume, 1979). A second difficulty with peak acceleration is its weak dependence on source strength; at least for potentially damaging earthquakes, peak acceleration at some fixed distance can be expected to "saturate" for exactly the same reasons that the magnitude scales m_b, M_L, and M_S also saturate (e.g., Hanks, 1979b; Hanks and Kanamori, 1979). Still another difficulty is the large scatter that exists in any reasonably large peak acceleration data set, even through very small ranges in hypocentral distance and earthquake magnitude (e.g., Seekins and Hanks, 1978). Because of these problems, it came as some surprise to us that peak acceleration (a_{max}) correlated so strongly with a_{rms} over $0 \leq t - R/\beta \leq T_d$ at all distances and azimuths for the San Fernando earthquake (McGuire and Hanks, 1980, Figure 6).

Figure 5 shows a similarly strong correlation between a_{max} and a_{rms} for the seven Oroville aftershocks, plotted on a linear scale. The strong correlation between a_{max} and a_{rms} and the sharply defined bounding ratios of $2 \lesssim a_{max}/a_{rms} \lesssim 3$ suggest a_{max} is simply the last amplitude point in a Gaussian distribution of acceleration amplitudes, removed from the mean (of zero) by two to three standard deviations. In the next section, we verify directly with frequency-of-occurrence counts that acceleration amplitudes within $0 \leq t - R/\beta \leq T_d$ indeed distribute in a nearly Gaussian manner; here we explore the predictability of peak accelerations on this basis.

According to Vanmarcke and Lai (1977), ground acceleration time histories that are stationary, random, and Gaussian in a time interval s_o will be characterized by

$$\frac{a_{max}}{a_{rms}} = \sqrt{2\ln\left(\frac{2s_o}{T_o}\right)} \quad , \tag{5}$$

where the a_{max} so determined should be exceeded once on the average--or, with a probability of e^{-1}, will not be exceeded--during s_o; here T_o is "the predominant period of the earthquake motion". In the framework of this study, we equate s_o with the faulting duration T_d, for which the record a_{rms} values are calculated and for T_o take the reciprocal of f_{max}, the highest frequency passed by the attenuation operator or the accelerograph. Equation (5) then becomes

$$\frac{a_{max}}{a_{rms}} = \sqrt{2\ln\left(\frac{2Q\beta}{\pi f_o R}\right)} \tag{6a}$$

or

$$\frac{a_{max}}{a_{rms}} = \sqrt{2\ln\left(\frac{2 f_{max}}{f_o}\right)} \quad . \tag{6b}$$

Plainly, some highly restrictive assumptions are implicit in (5) and (6), the discussion of which we delay in order to investigate whether or not this estimate of a_{max}/a_{rms} works.

Figure 6 plots the a_{max}/a_{rms} data for each of our three principal data sets. Figure 6a is for the seven Oroville aftershocks. Since virtually all of the observations are written at much the same distance (10 to 15 km), we have plotted observed values of a_{max}/a_{rms} versus f_o for each of the seven earthquakes. The triangles pointing horizontally and connected by the long-dashed line are the values predicted from equation (6b) with f_{max} = 25 Hz. The range in f_o for these seven events is not great, and the range in

the theoretical a_{max}/a_{rms} is much less; even so, with the exception of aftershock B, the median values of the observations (connected by the short-dashed line) track the trend of the theoretical prediction. In every instance, the observed a_{max}/a_{rms} is within ± 30 percent of the theoretical prediction.

Typically, however, the median values are lower than the predicted values by 10 to 15 percent; all of this effect can be attributed to our using Volume II (equally spaced data) peak accelerations, which generally are 10 to 20 percent smaller than peak accelerations scaled from Volume I data (unequally spaced, uncorrected for instrument response). Indeed, some care should be exercised in the use of peak accelerations taken from equally spaced representations of short-duration, high-frequency accelerograms such as those for the Oroville aftershocks; in three cases, all at DWR, the Volume II a_{max} was a factor of 2 or more lower than the Volume I a_{max} (in these cases, the Volume I datum was used).

Similarly, Figure 6b plots a_{max}/a_{rms} observations for the San Fernando earthquake as a function of distance. The theoretical prediction is from equation (6a), with Q = 300, β = 3.2 km/sec, and f_o = 0.1 Hz (Berrill; 1975; McGuire and Hanks, 1980). In this case, the observed ratios are all within ± 50 percent of the theoretical estimate. Generally speaking, a_{max}/a_{rms} decreases with increasing distance, in accord with the theoretical estimate, but here the theoretical estimate is slightly less (by 5 to 10 percent) than what might be a median observed value as a function of distance.

Finally, Figure 6c presents observed and theoretical values of a_{max}/a_{rms} for the other moderate-to-large California earthquakes. For this data set there are large variations in both f_o and R (Table 1), so Figure 6c plots the record estimate versus the model estimate (equation (6a)

evaluated for appropriate f_o, R, Q, and β). Again, the observations agree with the theoretical estimate to ± 50 percent in every instance, more of the observations than not being greater than the prediction.

To explore further the predictive value of (6), we estimate the $M_L \geq 4$ peak acceleration sets at close distances of Hanks and Johnson (1976) and Seekins and Hanks (1978) by combining equations (1) and 6a):

$$a_{max} = \left[0.85 \frac{(2\pi)^2}{106} \frac{\Delta\sigma}{\rho R^{3/2}} \sqrt{\frac{Q\beta}{\pi f_o}}\right] \sqrt{2 \ln \left(\frac{2Q\beta}{\pi f_o R}\right)} \qquad (7)$$

To evaluate (7), we set $\Delta\sigma$ = 100 bars, consistent with the results of the last section ($\Delta\sigma$ is known for some but not all of the earthquakes represented in Figure 7), and set R = 10 km, nominally consistent with the observations. All magnitudes for these earthquakes are M_L, except for the two largest which are M_S. Again for the purposes of evaluating (7), we treat the abscissa as moment magnitude M (Hanks and Kanamori, 1979). Thus M_o is determined by

$$\log M_o = 1.5\ M + 16.0 \qquad (8)$$

from which f_o for each M_o can be determined by the constant stress drop relation (Hanks and Thatcher, 1972)

$$\Delta\sigma = 100 \text{ bars} = 8.47 \frac{M_o f_o^3}{\beta^3} \qquad (9)$$

The numerical result of these operations is shown as the heavy solid curve in Figure 7. We have chosen not to plot (7) for M < 4 (or plot the M_L < 4 data of Hanks and Johnson (1976) and Seekins and Hanks (1978)) because as f_o approaches f_{max} equation (5), which assumes at least several cycles of

ground motion, is no longer valid. Below M = 4, faulting durations need be more than 0.1 sec or so. Neither have we plotted (7) for M > 6.5, for reasons discussed below.

The two light solid curves are an evaluation of the expression of Joyner et al (1981):

$$\log a_{max} = 1.76 + 0.28\,M - \log R - 0.00255\,R + 0.27P \qquad (10)$$

where we have set P=0 for 50 percent probability of exceedance. The upper curve is evaluated at R = 7.3 km (zero horizontal distance to the epicenter or faulting surface); the lower curve is for R = 10 km. Note that we give the relation of Joyner et al (1981) in cm/sec^2, where they give it in units of 980 cm/sec^2; R is measured in km. The constants in (10) are determined from a regression analysis on peak accelerations recorded at distances out to several hundred km for earthquakes with $5.0 \leq M \leq 7.7$.

Also shown in Figure 7 is the relation of Donovan (1973)

$$\log a_{max} = 3.12 + 0.25\,M - 1.52 \log (R + 25) \qquad (11)$$

evaluated at R = 0 and R = 10 km (light dashed lines). Here we have taken M for magnitude, and R is a "closest" distance in km. Donovan (1973) does not detail the range of validity for (11); we plot it for $5 \leq M \leq 7\ 1/2$.

In the range of mutual validity, $5.0 \leq M \leq 6.5$, the empirical relations of Donovan (1973) and Joyner et al (1981) and the theoretical relation developed here are remarkably similar; the several dependences of $\log a_{max}$ on M are

nearly identical. For our model, the a_{max} dependence on M_o

$$a_{max} = 0.45 \left[\sqrt{\frac{Q}{\pi}} \frac{(\Delta\sigma)^{5/6}}{\rho R^{3/2}} \right] M_o^{1/6} \sqrt{2 \ln \left[\left(\frac{4.10}{\pi R (\Delta\sigma)^{1/3}} \right) M_o^{1/3} \right]} \quad (12)$$

works out to be almost exactly

$$a_{max} \sim M_o^{1/5} \quad (13)$$

for $4 \leq M \leq 6.5$. With the use of (8), this becomes

$$\log a_{max} \sim 0.30\, M \text{ (or } M_L) \quad (14)$$

The coefficient on M is 0.25 for the Donovan (1973) relation and 0.28 ± 0.04 for the Joyner et al (1981) relation. Differences in absolute values for log a_{max} of 0.2 to 0.3 units can (and do) arise through various definitions of the "zero" or closest distance, a problem not readily amenable to resolution given the scatter of comparable magnitude in the observations for any M at close distances. In view of the limitations of the data set in Figure 7, its natural scatter, and the real variations in R for the observations that have been suppressed with R = 10 km, all of these relations "fit" the observations about as well as can be expected for $5 \leq M \leq 6\ 1/2$.

All of these relations, however, either do or would underestimate the Hanks and Johnson (1976) data for $4 \leq M \leq 5$, by factors of 2 to 3. Our theoretical expression agrees well with the the $M_L \geq 4$ Oroville aftershock mean-value a_{max} data, however, and we suspect that these are the more compelling observational constraints. The data set of Hanks and Johnson (1976) was compiled simply from the largest peak accelerations then known at R = 10 km, without knowledge of what might be an appropriate mean value at $M < 5$. Nevertheless, there remains a possibility that the log a_{max} dependence on M ($4 \leq M \leq 6\ 1/2$) at close distances might be somewhat less than

that given either by our model or the empirical relations of Donovan (1973) and Joyner et al (1981).

Of greater concern is the M dependence of a_{max} at close distances for $M > 6\ 1/2$.. In the $M > 6\ 1/2$ and $R \lesssim 10$ km space, the observations are very sparse, and both the assumed functional forms of the empirical studies and our theoretical model are of uncertain validity. Nevertheless at $M = 6.5$ and $R = 10$ km, we are impressed by the convergence of observational results, theoretical expectation, and popular consensus: peak accelerations in the vicinity of 1/2 g (±50 percent) will be the norm for $M \simeq 6\ 1/2$ earthquakes at close distances, not the exception (e.g. Donovan, 1973; Hanks and Johnson, 1976; Boore et al, 1980; Campbell et al, 1980; Joyner et al, 1981; and the results of this study). But what may we expect for greater M?

In the model presented here, all the magnitude dependence of peak acceleration is a function of duration alone: In view of the reasonable match of the observations to theoretical expectation, at least for $4 < M < 6\ 1/2$, we conclude that larger earthquakes have larger peak accelerations because they last longer, not becuase they are intrinsically more powerful, an hypothesis advanced previously by Hanks and Johnson (1976) without the benefit of equation (7). Thus, at close distances, if the duration of <u>strongest</u> motion cannot increase beyond a certain value (perhaps, for reference, 10 to 20 seconds), then neither can the peak acceleration, if we can always count on finding it in the strongest motion portion of the record. Specfically, larger magnitude earthquakes will be associated with fault lengths that become progressively larger than $R \simeq 10$ km, which then would be the distance of closest approach. Even though the faulting duration of such an event will continue to increase, the a_{rms} at any "close" site over that duration will <u>decrease</u> with increasing duration, because of the greater distances the

radiation from the outlying faulting segments must travel to that site. But we do not expect a_{max} to decrease for such events if it is caused by faulting on the closest segment, taking it to be the source of the strongest motion. On the other hand, a_{max} need not increase by much above ~ 1/2 g for $M > 6\ 1/2$ at close distances, and we expect it will not, the linear increase in log a_{max} above $M = 6.5$ assumed in the empirical relations of Donovan (1973) and Joyner et al (1981) notwithstanding.

THE GAUSSIAN CHARACTER OF ACCELERATION TIME HISTORIES

The results of the two previous sections suggest that there is considerable evidence that the high-frequency strong ground motion that arrives as direct shear waves is finite-duration ($0 \leq t-R/\beta \leq T_d$), band-limited ($f_o \leq f \leq f_{max}$) white, Gaussian noise. The agreement between the a_{max}/a_{rms} ratios estimated on this basis with a variety of observations, while far from perfect, nevertheless provides a stringent test of the assumptions implicit in equations (5), (6), and (7), given any scatter at all in the observations not explicitly accounted for in the model and uncertainties in the parameters used in the model. In particular, we have estimated to ± 50 percent, most of the time, the last amplitude point (a_{max}) in almost 400 series of several hundred to more than a thousand acceleration amplitudes, depending on the record. It is unlikely that this coincidence would materialize if any of the above characterizations were seriously in error, although we have previously noted the potential trade offs between stress drops and high-frequency spectral decay rates. In this section, we verify the Gaussian character directly with frequency-of-occurrence plots of the amplitude data.

Figues 8a and 8b demonstrate that acceleration amplitudes within the shear-wave arrival window ($0 \leq t-R/\beta \leq Td$) distribute in a very nearly Gaussian manner. Figure 8a shows these amplitude distributions plotted on normal probability paper for one component of motion from each of our three principal sets of data, those for the San Fernanado earthquake, the other moderate-to-large California earthquakes, and the Oroville aftershocks. The abscissa in each case is acceleration amplitude normalized to a_{rms} for that record. In Figure 8b are similar results for <u>all</u> of the San Fernando earthquake records analyzed by McGuire and Hanks (1980), amplitudes again being normalized to a_{rms} for each record of the set. Similar data for the entire Oroville aftershock data set (Table 2) and the other moderate-to-large California earthquakes (Table 1) overlap the symbols in Figure 8b to the point where the three sets could not be distinguished at the given symbol size; they are not shown here. Both individually and collectively, then, these figures demonstrate that acceleration amplitudes in the shear-wave arrival window are distributed in a manner only trifling different from Gaussian, but this should come as no great surprise, in view of our ability to estimate so well the <u>last</u> amplitude point (the peak acceleration) under the Gaussian assumption.

SUMMARY AND CONCLUSIONS

From an analysis of more than 300 components of ground acceleration of 16 earthquakes of magnitude $4.0 \leq M \leq 7.7$ at distances of $10 \leq R \leq 100$ km in this study and McGuire and Hanks (1980), high-frequency strong ground motion is, to a very good approximation, band-limited ($f_o \leq f \leq f_{max}$), finite-duration ($0 \leq t - R/\beta \leq T_d$), white, Gaussian noise. Its rms value is fixed by the

single earthquake source parameter $1/\sqrt{\tau_0}$ (or equivalently $M_0^{1/6}$), since for all of these events $\Delta\sigma$ has been estimated from record estimates of a_{rms} to be nearly equal to 100 bars. Although we have made no formal statistical analysis of the matter, with these parameters and equally simplistic wave propagation effects, one can model estimates of a_{rms} that agree within a factor of 2 of the record estimates about 85 percent of the time. These results are of great significance for the rational construction of synthetic accelerograms, at least for $M \leq 6\ 1/2$ earthquakes.

On this same basis, one can predict peak accelerations with comparable accuracy. The magnitude-dependence of peak acceleration determined empirically by Joyner et al (1981) for $5.0 \leq M \leq 7.7$ is remarkably similar to that determined by equations (7) and (8) for $4.0 \leq M \leq 6\ 1/2$, the magnitude coefficient being 0.28 in the first case and 0.30 in the second. This magnitude dependence of peak acceleration is a function of faulting duration alone; at a fixed, close distance larger earthquakes have larger peak accelerations only because they last longer, not because they are intrinsically more powerful. Even from just a seismological point of view, then, faulting duration is an important ground motion parameter. Should "effective peak acceleration" continue to want for a "precise definition in physical terms," we recommend that it be a_{rms} for the time interval $0 \leq t - R/\beta \leq T_d$.

Seismologically, these results are no less fascinating. Of considerable significance is the result that the earthquake stress drops as determined by a_{rms} are very nearly equal to 100 bars; estimates for any of the 16 earthquakes of interest here vary over ± a factor of 2, not 2 orders of

magnitude. While all of these are California earthquakes, they occurred in a variety of tectonic settings and spanned a considerable range in source strength; had past experience in stress-drop determinations been the measure of expectation, there would be no reason why these events would have so nearly the same stress drops. The results reported here, however, are the only available stress drops determined by a_{rms}, and they may be more akin to a dynamic stress drop than an average static stress drop, in view of the high-frequency character of the motion from which they are derived. Only further study of a larger class of earthquakes will reveal whether or not a wider range of a_{rms}-determined stress drops will materialize and whether or not the offsetting relation between $\Delta\sigma$ and γ, as postulated earlier, might exist. Similarly, Table 2 suggests that a_{rms} is a remarkably - and surprisingly -- stable measure of high-frequency ground motion, no matter what purpose to which it is put; further study of this phenomenom is also warranted.

While scattering mechanisms undoubtedly contribute some component to the chaotic but stochastically well-behaved character of high-frequency strong ground motion, we believe for two reasons that these properties are fundamentally due to properties of the source, not path. First, there is no distance-dependence of the scatter in the a_{max}/a_{rms} ratio for the San Fernando earthquake; the acceleration time histories are as white, Gaussian, and random at 20 km as at 120 km, although the bandwidth narrows with increasing distance. Secondly, in the case of the 0103 aftershock of the Oroville earthquake, Boatwright (1981) was able to identify and locate 5 sub-events within the ~ 0.7 second faulting duration. This complexity is plainly a function of the source, not path; indeed, had there been much phase incoherence at all along the propagation paths, it is unlikely that this sub-event analysis would have been possible.

On this matter as well, further study is plainly indicated, but the results of this study suggest that the stress differences that develop in the course of crustal faulting, giving rise to the acceleration time histories studied here, are also very well-behaved, both in the average stress release through the characteristic source volume and in the character of stress differences that develop across smaller dimensions. In particular, given the white, random, and Gaussian character of acceleration time histories for $0 < t-R/\beta \leq T_d$, the linear relation of Hanks and Johnson (1976) between dynamic stress differences for localized and isolated events in the source region and acceleration amplitudes at R should allow for a straightforward mapping of the latter into the former. These results should be of value in the further development of the relationships that might exist between frequency-of-occurrence statistics (b-values), average earthquake stress drops ($\Delta\sigma$) and rate of high-frequency spectral decay in the far-field (γ) - and how any or all of them might be related to the distribution and spectral composition of quasi-static stress differences existing along active crustal fault zones (e.g. Nur, 1978; Hanks, 1979a; Andrews, 1980; von Seggern, 1980).

Finally, it seems almost certain that inhomogeneities in the quasistatic tectonic stress field that gives rise to the earthquake or inhomogeneities in stress differences that develop dynamically in the course of crustal faulting -- or most likely both effects -- are an intrinsic characteristic of crustal earthquakes. $M \approx 4$ earthquakes appear to be as complicated at periods ≈ 0.1 sec as $M \approx 6$ earthquakes are at periods ≈ 1 sec and $M \approx 8$ earthquakes are at periods ≈ 10 sec. Indeed, earthquake "complexity" may be a self-similar charcteristic of crustal earthquakes. In view of the heterogeneous morphology

of active crustal fault zones, so readily apparent in their en-echelon, locally discontinuous character as observed both geologically (Wallace, 1968; Tchalenko, 1970) and seismically (Eaton, 1970; Bakun, 1980), this "complexity" character of crustal earthquakes is probably to be expected.

References

Andrews, D.J. (1980). A stochastic fault model, 1. static case, J. Geophy. Res. 85, 3867-3877.

Applied Technology Council (1978). Tentative provisions for the development of seismic regulations for buildings, National Bureau of Standards Special Publication 510, pp. 506.

Bakun, W.H., R.M. Stewart, C.G. Bufe, and S.M. Marks (1980) Implication of seismicity for failure of a section of the San Andreas fault. Bull. Seism. Soc. Am. 70, 185-201.

Boatwright, J. L. (1981) Quasi-dynamic models of simple earthquakes: application to an aftershock of the 1975 Oroville, California earthquake, Bull. Seism. Soc. Am., 71, 69-94.

Berrill, J.B. (1975). A study of high-frequency strong ground motion from the San Fernando earthquake, Ph.D. Thesis, California Institute of Technology, Pasadena.

Blume, J.A. (1979). On instrumental versus effective acceleration, and design coefficients, Proceedings of the 2nd U.S. National Conference on Earthquake Engineering, 868-882, Earthquake Engineering Research Institute, Berkeley.

Bolt, B. A. (1978). The local magnitude M_L of the Kern County earthquake of July 21, 1952, Bull. Seism. Soc. Am. 68, 513-515.

Boore, D. M., W. B. Joyner, A. A. Oliver III, and R. A. Page (1980). Peak acceleration, velocity, and displacement from strong-motion records, Bull. Seism. Soc. Am. 70, 305-321.

Brune, J.N. (1970). Tectonic stress and the spectra of seismic shear waves from earthquakes, J. Geophys. Res. 75, 4997-5009.

Brune, J.N. (1971). Correction, J. Geophys. Res. 76, 5002.

Joyner, W.B., D.M. Boore, and R.L. Porcella (1981). Peak horizontal acceleration and velocity from strong motion records including records from the 1979 Imperial Valley, California, earthquake, U.S. Geol. Survey Open-file Report 81-365.

Kanamori, H. and D.L. Anderson (1975). Theoretical basis of some empirical relations in seismology, Bull. Seism. Soc. Am. 65, 1073-1096.

Kanamori, H. and P.C. Jennings (1978). Determination of local magnitude, M_L, from strong-motion accelerograms, Bull. Seism. Soc. Am. 68, 471-485.

Kudo, K. (1978). The contribution of Love waves to strong ground motions, Proceedings of the Second International Conference on Microzonation for Safer Construction - Research and Applications, 765-776.

McCann, M. W. (1980). rms acceleration and duration of strong ground motion, Dept. Civ. Engg. Rept. No. 46, Stanford University.

McGuire, R.K. and T.P. Barnhard (1979). Four definitions of strong motion duration: their predictability and utility for seismic hazard analysis, U.S. Geol. Survey Open-file Report 79-1515.

McGuire, R.K. and T.C. Hanks (1980). RMS accelerations and spectral amplitudes of strong ground motion during the san Fernando, California earthquake, Bull. Seism. Soc. Am. 70, 1907-1919.

Nur, A. (1978). Nonuniform friction as a physical basis for earthquake mechanics, Pure Appl. Geophysics 116, 964-989.

Schnabel, P. B. and H. B. Seed (1973). Accelerations in rock for earthquakes in the western United States, Bull. Seism. Soc. Am. 63, 501-516.

Seekins, L.C. and T.C. Hanks (1978). Strong motion accelerograms of the Oroville aftershocks and peak acceleration data, Bull. Seism. Soc. Am. 68, 677-690.

Seekins, L.C., D.P. Hill, and T.C. Hanks (1978). Shear-wave velocity structure near Oroville, California, Bull. Seism. Soc. Am. 68, 691-698.

Swanger, H.J. and D.M. Boore (1978a). Simulation of strong-motion displacements using surface-wave modal superposition, Bull. Seism. Soc. Am. 68, 907-922.

Swanger, H.J. and D.M. Boore (1978a). Importance of surface waves in strong ground motion in the period range 1 to 10 seconds, Proceedings of the Second International Conference on Microzonation for Safer Construction - Research and Application, 1447-1457.

Tchalenko, J.S. (1970). Similarities between shear zones of different magnitudes, Geol. Soc. Am. Bull. 81, 1625-1640.

Thatcher, W. and T.C. Hanks (1973). Source parameters of sourthern California earthquakes, J. Geophys. Res. 78, 8547-8576.

Tocher, D., (1959). Seismic history of the San Francisco region, San Francisco Earthquakes of March 1957, Calif. Div. Mines Geol. Spec. Rep. 57.

Trifunac, M. D. (1976). Preliminary analysis of peaks of strong earthquake ground motion-dependence of peaks on earthquake magnitude, epicentral distance, and recording site conditions, Bull. Seism. Soc. Am. 66, 189-219.

Trifunac, M.D. and J.N. Brune (1970). Complexity of energy release during the Imperial Valley, California, earthquake of 1940, Bull. Seism. Soc. Am. 60, 137-160.

Trifunac, M.D. and F.E. Udwadia (1975). Parkfield, California, earthquake of June 27, 1966: a three-dimensional moving dislocation, Bull. Seism. Soc. Am. 64, 511-533.

Tucker, B.E. and J.N. Brune (1973). Seismograms, S-wave spectra, and source parameters for aftershocks of San Fernando earthquake, in San Fernando, California, Earthquake of February 9, 1971, Vol. III (Geological and Geophysical Studies), 69-122, U.S. Dept. Commerce

Vanmarcke, E.H. and S.P. Lai (1977). Strong-motion duration of earthquakes, Dept. of Civil Eng. Pub. No. R77-16, Massachusetts Institute of Technology, Cambridge.

von Seggern, D. (1980). A random stress model for seismicity statistics and earthquake prediction, Geophys. Res. Lett. 70, 637-640.

Wallace, R.E. (1968). Notes on stream channels offset by the San Andreas fault, Southern Coast Ranges, California, Proceedings of Conference on Geologic Problems of San Andreas Fault System, Stanford Univ. Publ. Geol. Sci. 11, 6-21.

Table 1

Earthquake Source Parameters and Strong-Motion Accelerograms

Earthquake date; magnitude	M_o dyne-cm		$\Delta\sigma$ bars	$T_d = f_o^{-1}$ sec	Accelerograms ID (CIT)	S-arrival Sec	R km	References
Long Beach Mar. 11, 1933; M_L=6.3	2 1/2 x 10^{25}		10	10	B021 V314 V315	1.0 1.0 0.5	50 55 20	Thatcher and Hanks (1973) Kanamori and Anderson (1975)
Imperial Valley May 19, 1940; M_S=7.1, M_L=6.4	3 x 10^{26}		50	12	A001[1]	0.7	20	Trifunac and Brune (1970)
Kern County July 21, 1952; M_S=7.7, M_L=7.2	2 x 10^{27}		60	20	A003 A004 A005 A006	11.7 2.7 6.2 8.5	130 40 90 120	Kanamori and Anderson (1975) Hanks (1976, 1979a) Kanamori and Jennings (1978) Bolt (1978)
Wheeler Ridge Jan. 12, 1954; M_L=5.9	3 x 10^{24}		6	5	B031	4.0	40	Thatcher and Hanks (1973)
San Francisco[2] Mar. 22, 1957; M_L=5.3	1 x 10^{24}		50	1.7	A013 A014 A015 A016 A017	0.6 1.1 1.0 0.5 0.3	20 20 15 20 30	Tocher (1957)
Parkfield June 28, 1966; M_S=6.4, M_L=5.5	3 1/2 x 10^{25}		17	8	B033 B034 B035 B036 B037	1.6 4.6 1.2 1.9 1.1( )	20 20 25 25 30	Kanamori and Anderson (1975) Trifunac and Udwadia (1975)
Borrego Mountain[3] Apr 9, 1968; M_S=6.7, M_L=6.4	7 x 10^{25}	A B	17 140	10 5	A019 A020	6.6 7.1	60 100	Hanks and Wyss (1972) Kanamori and Anderson (1975) Burdick and Mellman (1976) Heaton and Helmberger (1977)
Lytle Creek[4] Sept 12, 1970; M_L=5.4	1 x 10^{24}		30	2	W334 W335 W338	0.2 0.0 0.0	12 18 25	Hanks et al (1975)

1 Analysis of this record performed with ρ=2.5 gm/cm^3, β=2.5 km/sec, and Q=200
2 M_o determined from log M_o = 1.5 M_L + 16.0; f_o determined from aftershock dimension r = 2km
3 Model A according to interpretations of Hanks and Wyss (1972) and Kanamori and Anderson (1975); Model B according to Burdick and Mellman (1976)
4 M_o and f_o from unpublished data of T. C. Hanks

Table 2

a_{rms} – determined Stress Drop Estimates (bars) for Seven Oroville Aftershocks

Date	Origin Hr min	M_L	f_o (Hz)	2 N90W S00E	3 N85W S05W	OAP N90W S00E	1 N50E N00E	4 N35W S55W	5 S00E N90E	EBH N50E N00E	OMC N24W S66W	DJR N90E N00E	7 N90W S00W	DWR S00E N90E	6 S55E N35E	8 N90W S00E	9 N20W S70W	$\Delta\sigma^1$ arith. log
Aug 3	0103(A)	4.6	1.4		42	63	129	83	110	156	107			125				97
					38	27	114	103	135	143	117			91				87
Aug 3	0247(B)	4.1	1.9		S[2]	96	54	113	101	133	59			53				90
						45	83	97	106	71	122			37				86
Aug 6	0350(F)	4.7	1.3	121	123	185	186	96	167	171	248	344		304				173
				124	293	279	180	138	160	171	119	887		144				164
Aug 8	0700(K)	4.9	1.6			83	105	72	68	78		88	65	178	65			87
						56	178	82	73	138		200	62	83	95			82
Aug 16	0548(P)	4.0	3.0			45	164	58	70	107	106	190	70	101	123	53		97
						59	312	98	105	74	41	228	56	94	114	91		85
Sep 26	0231(T)	4.0	2.2			88	91	77	146	89	95	358			130	S	S	101
						74	110	104	153	89	81	258			83			98
Sep 27	2234(U)	4.6	2.2			320	176	175	204	178	142	474		184		278	155	195
						324	209	132	161	235	144	998		231		127	164	187

1 Excluding DJR and DWR
2 Denotes a record that did not clearly trigger on or before S-wave arrival

Table 3

Comparison of Normalized a_{rms} - determined stress drop estimates to normalized shear-wave radiation patterns for the Oroville aftershock 0231

Structure	Component	$\Delta\sigma/\overline{\Delta\sigma}$	1.76 $R_{\theta\phi}/\langle R_{\theta\phi}\rangle$
OMC	N24W	0.94	0.56
	S66W	0.80	0.96
CD6	S55E	1.29	1.03
	N35E	0.83	2.40
EBH	N90E	0.88	1.57
	N00E	0.88	0.30
CD5	S00E	1.45	0.16
	N90E	1.51	1.10
CD4	N35W	0.76	0.41
	S55W	1.03	1.08
OAP	N90W	0.87	1.50
	S00E	0.73	0.024
CD1	N90E	0.90	1.18
	N00E	1.09	0.43

Figure Captions

1. Transverse components of ground acceleration of the San Fernando earthquake for 15 seconds beginning with the S-wave arrival at the Seismological Laboratory (top) and the Athenaeum (bottom) of the California Institute of Technology in Pasadena; these sites are 36 and 40 km, respectively, from the hypocenter.

2. Peak displacements, velocities, and accelerations for the San Fernando earthquake along Profile 1 of Hanks (1975) are plotted from top to bottom on the left side of the figure. The crosses are the more transverse component of horizontal motion, the circles the more radial component. The arrival times of these phases with respect to S! (Hanks, 1975) are plotted on the right side of the figure. Note that the peak accelerations at all distances arrive within 10 seconds of S!.

3. The ratio of record/model a_{rms} for each source-station pair of Table 1 is plotted against earthquake stress drop.

4. Comparison of record a_{rms} to model a_{rms} for the source-station pairs of Table 1, (and Figure 3), when all model estimates are calculated with $\Delta\sigma$ = 100 bars.

5. a_{max} vs a_{rms} for the seven Oroville aftershocks (Table 2). In order to present this data on linear scales, four data pairs with $a_{rms} > 110$ cm/sec^2 are not included. Otherwise, there is one point for each source/station component pair in Table 2. Circles are bedrock sites, crosses are sedimentary sites, according to the classification of Seekins and Hanks (1978).

6. Record and model estimates of a_{max}/a_{rms}
   a. Oroville aftershocks, as a function of f_o
   b. San Fernando earthquake, as a function of R
   c. Other moderate-to-large California earthquakes, observed ratio as a function of theoretical ratio

7. The $M_L \geq 4$ peak acceleration data at R ≈ 10 km of Hanks and Johnson (1976) (solid symbols) and the Oroville aftershock mean-value peak accelerations (Seekins and Hanks, 1978) (open and half-filled circles for sediment and bedrock sites, respectively). The peak acceleration-magnitude relations at fixed close distances of Donovan (1973) and Joyner et al (1981), labeled JBP, are as shown for two choices of R. The numerical expression of the model developed in this study is labeled as such.

8. Acceleration amplitude frequency-of-occurrence counts, normalized to the record a_{rms} over $0 \leq t-R/\beta \leq T_d$
   a. individual components from the three principal data sets, the San Fernando earthquake, the other moderate-to-large California earthquakes, and the Oroville aftershocks
   b. all records for the San Fernando earthquake used by McGuire and Hanks (1980).

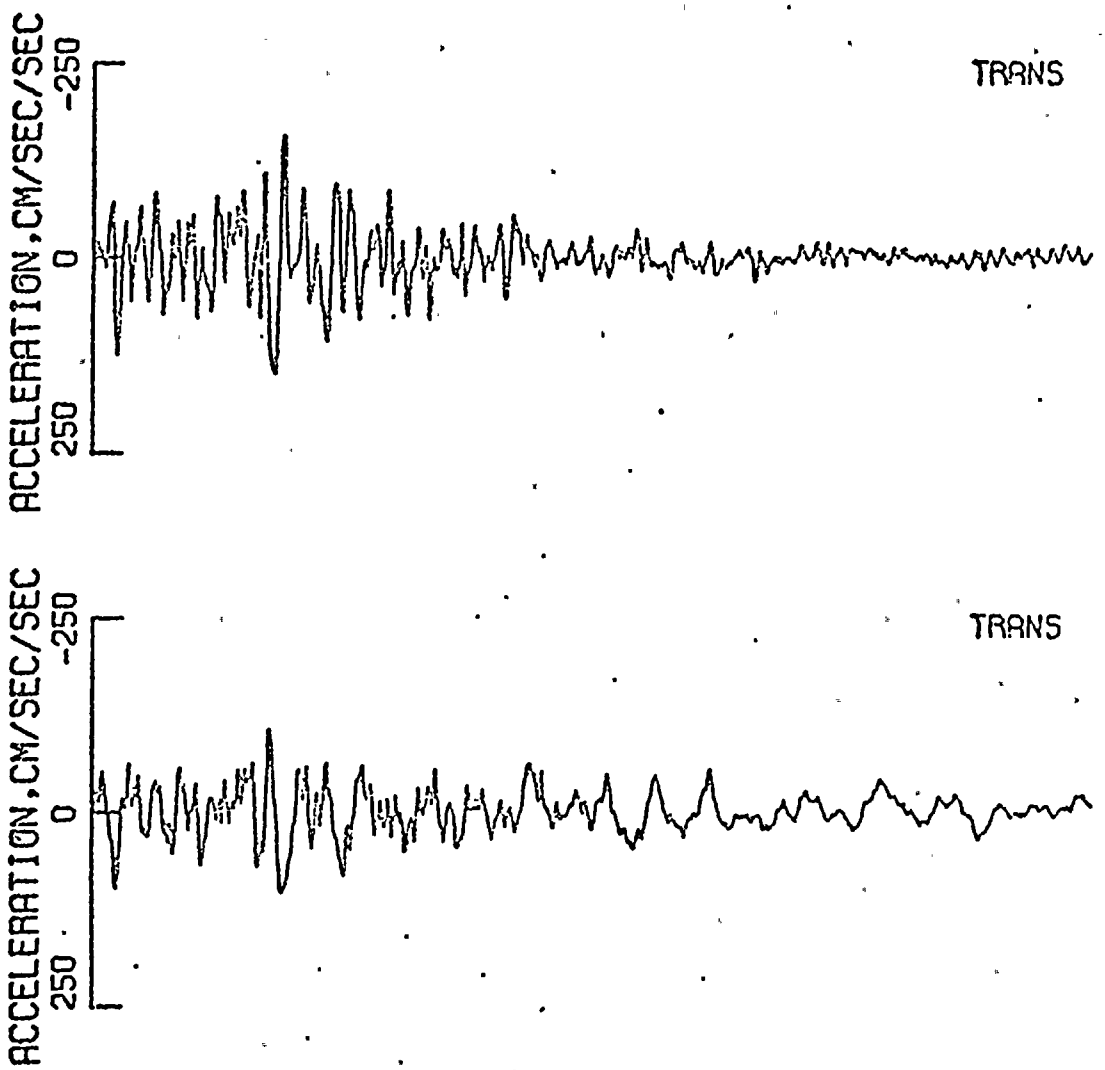
ACCELERATION,CM/SEC/SEC
-250
0
250
TRANS
ACCELERATION,CM/SEC/SEC
-250
0
250
TRANS

Fig 1

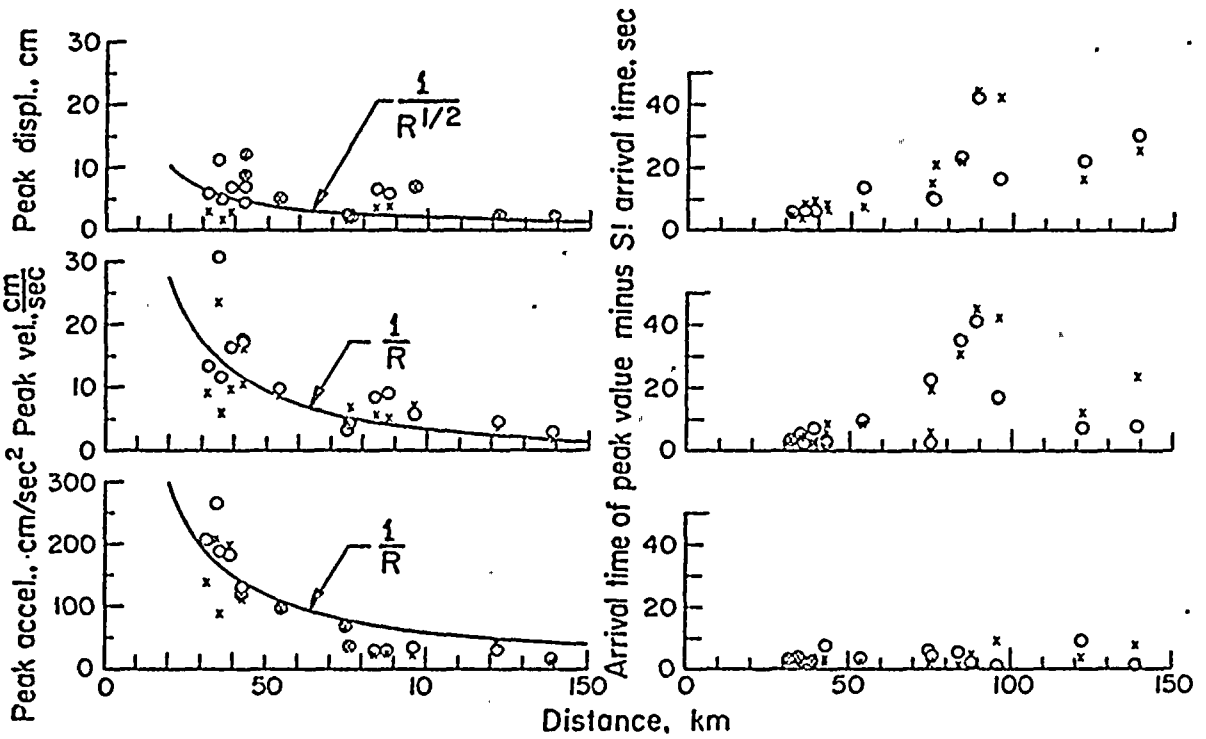
Peak displ., cm
Peak vel., cm/sec
Peak accel., cm/sec²
1/R^1/2
1/R
1/R
Arrival time of peak value minus S! arrival time, sec
Distance, km

Fig 2

Fig 3

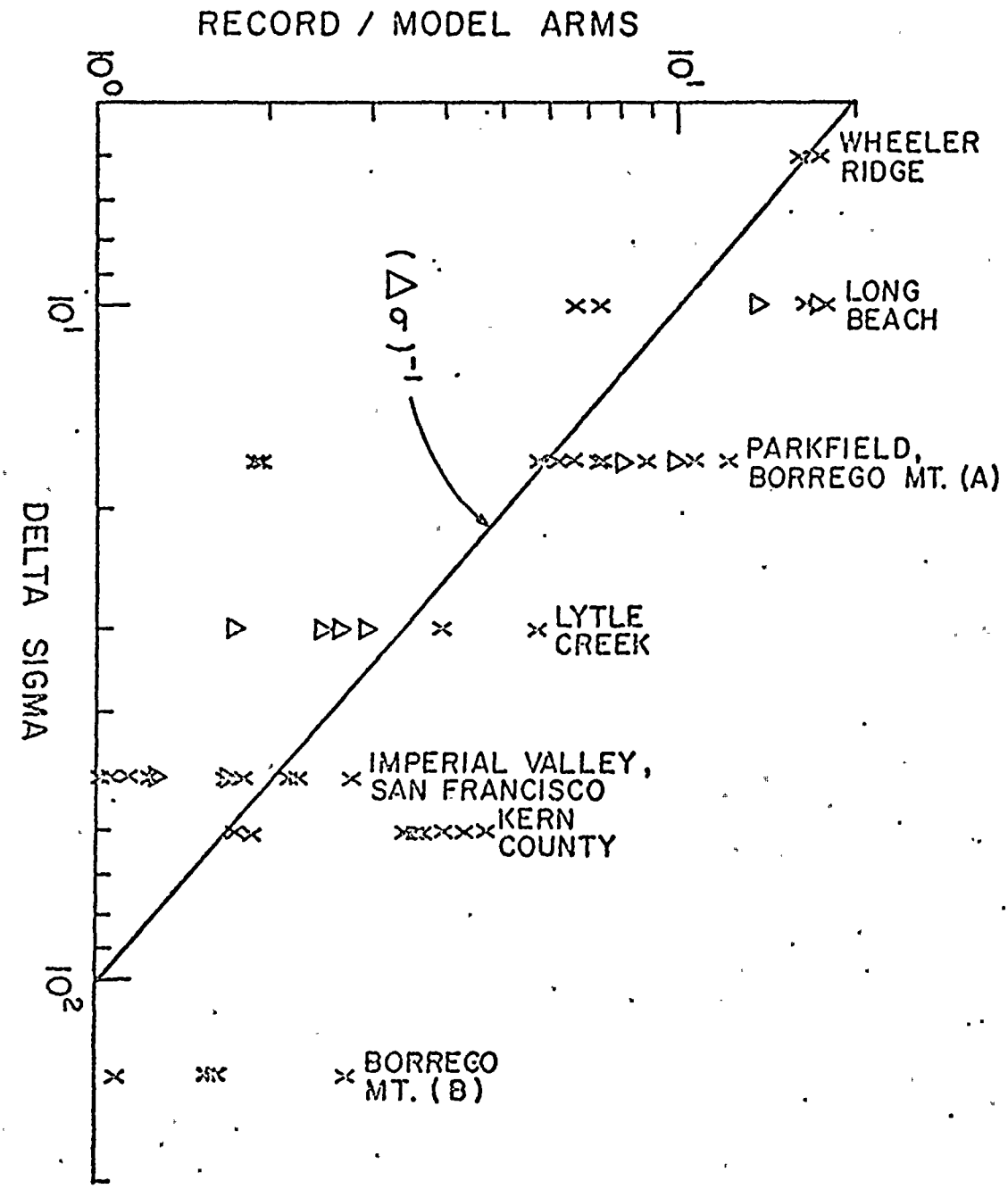
RECORD / MODEL ARMS
10^0
10^-
10^1
10^2
DELTA SIGMA
$(\Delta\sigma)^{-1}$
WHEELER RIDGE
LONG BEACH
PARKFIELD, BORREGO MT. (A)
LYTLE CREEK
IMPERIAL VALLEY, SAN FRANCISCO
KERN COUNTY
BORREGO MT. (B)

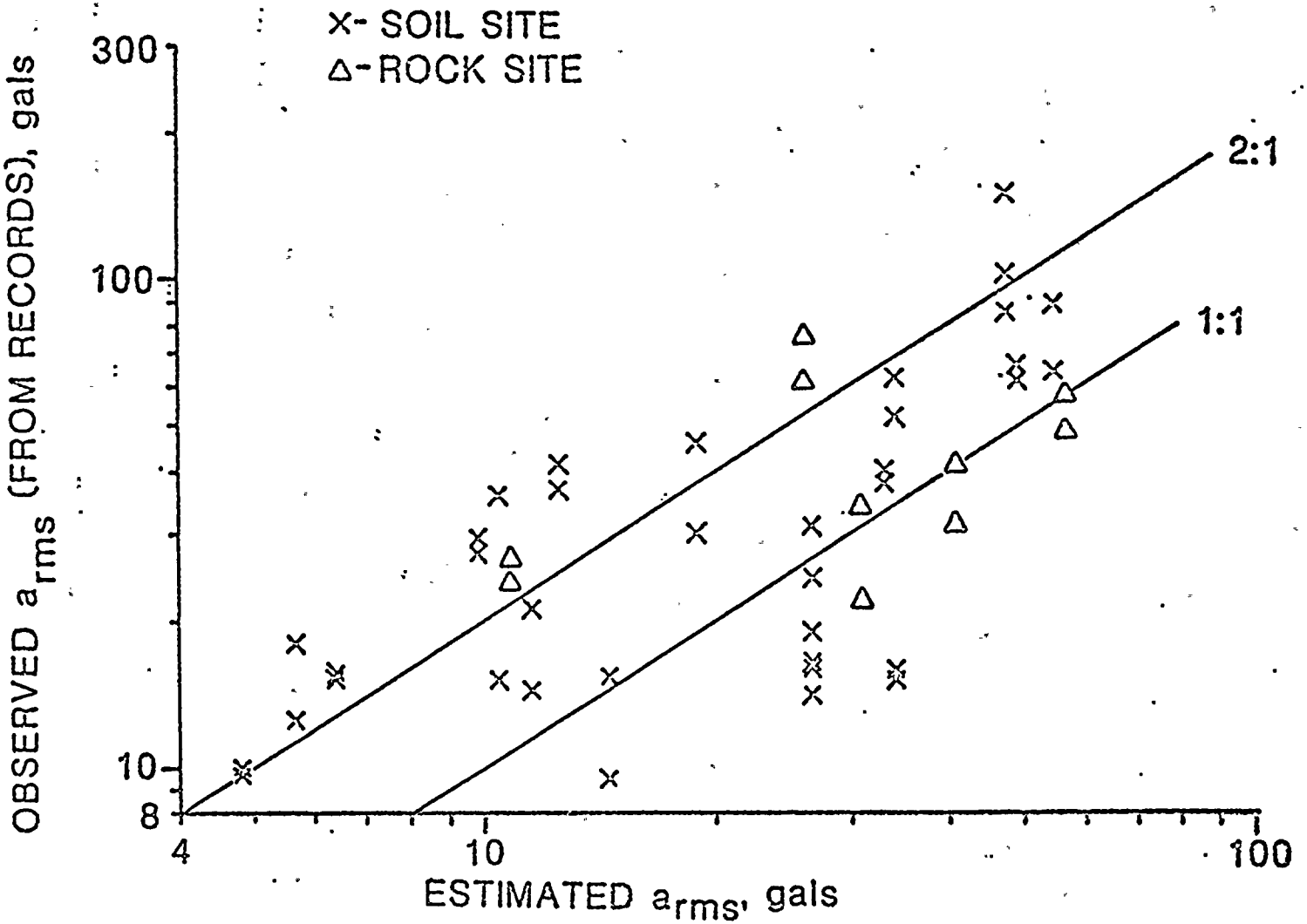
× - SOIL SITE
Δ - ROCK SITE
2:1
1:1
300
100
10
8
4
10
100
OBSERVED a_{rms} (FROM RECORDS), gals
ESTIMATED a_{rms}, gals

Fig 4

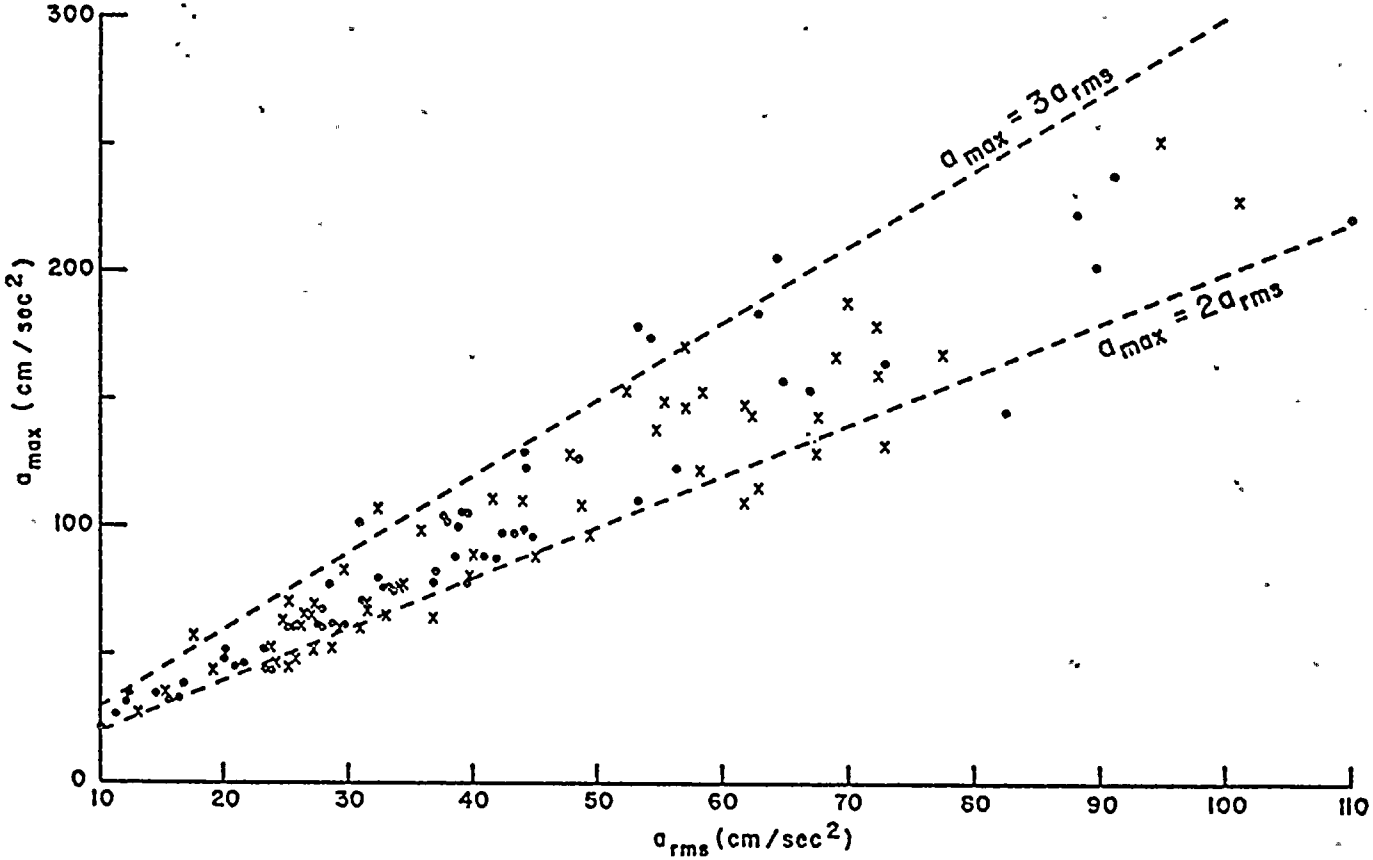
300
200
100
0
10
20
30
40
50
60
70
80
90
100
110
a_{max} (cm / sec^2)
a_{rms} (cm/sec^2)
$a_{max} = 3a_{rms}$
$a_{max} = 2a_{rms}$

Fig 5

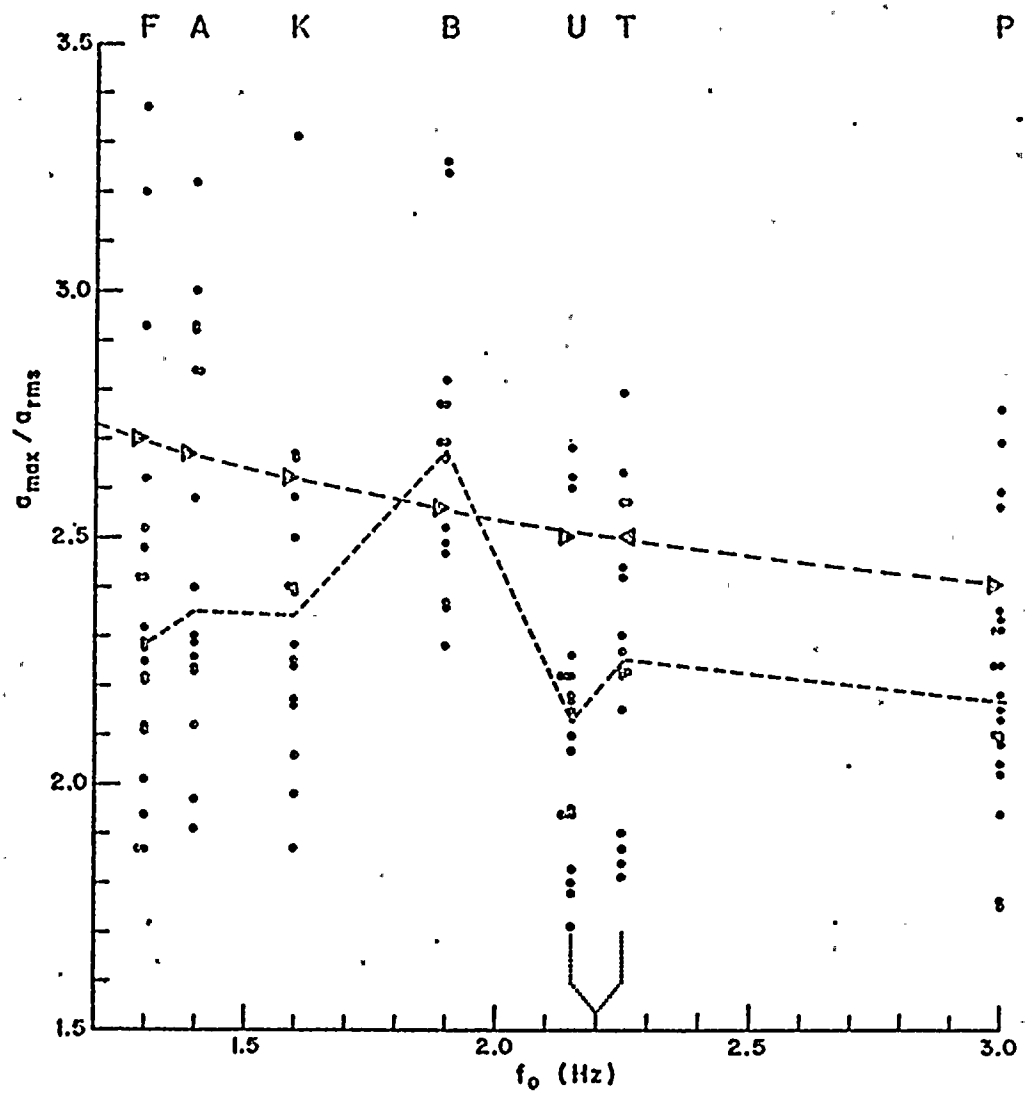

Fig 6a.

MAX./RMS. ACC. VS DISTANCE

SAN FERNANDO, CAL.

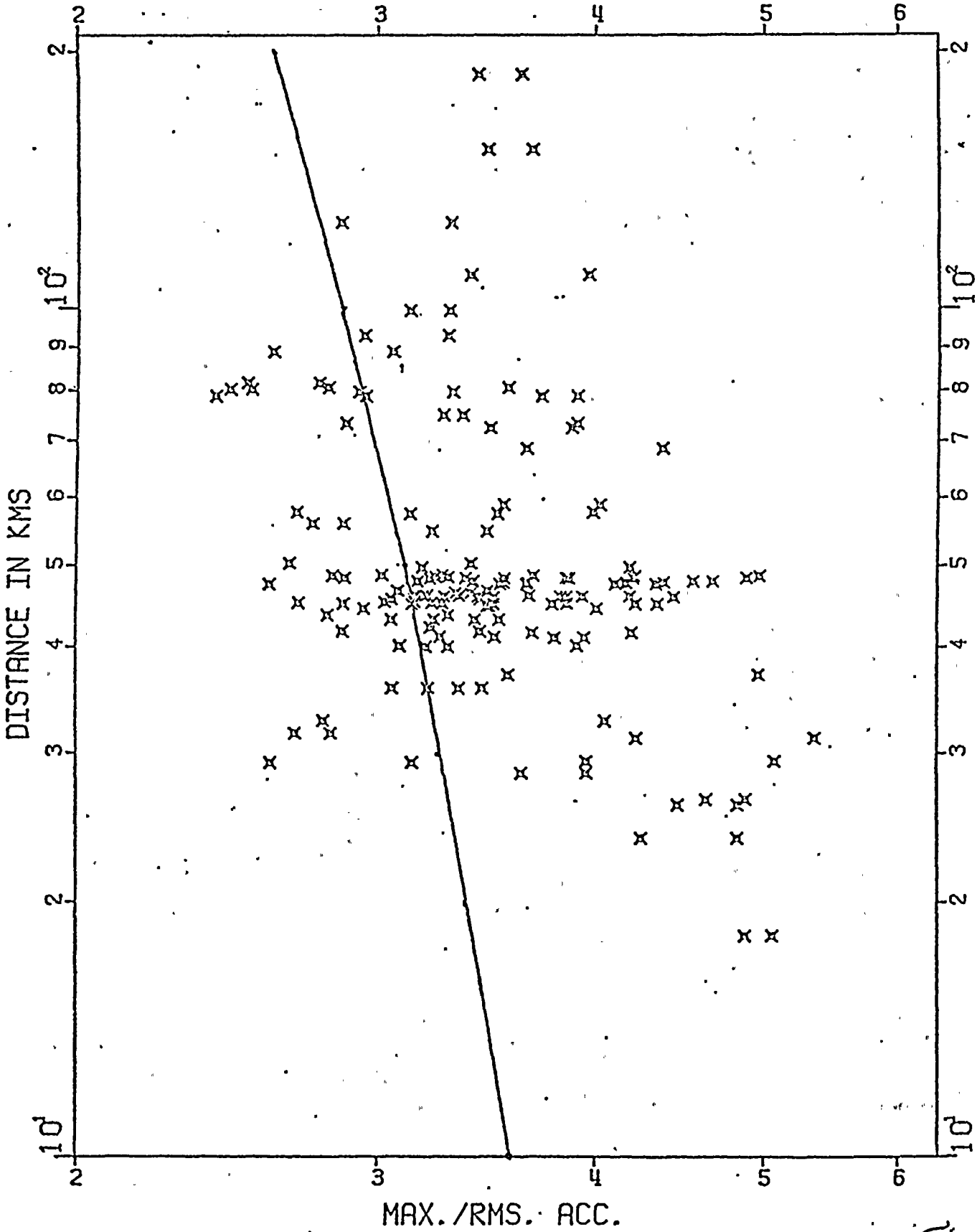

Fig 6b

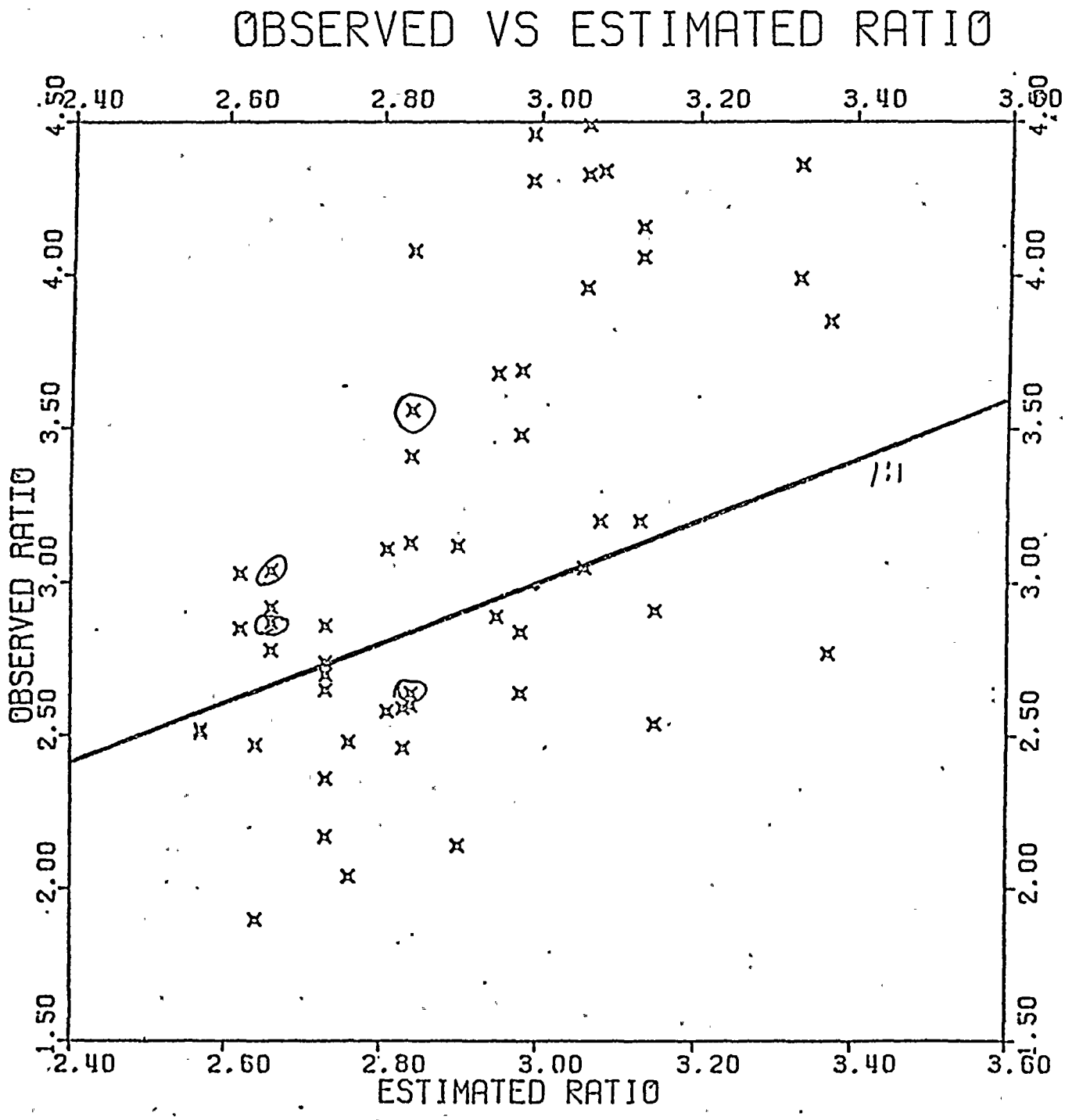

O = Borrego Mt "B"
(140 bars)

Fig 6c

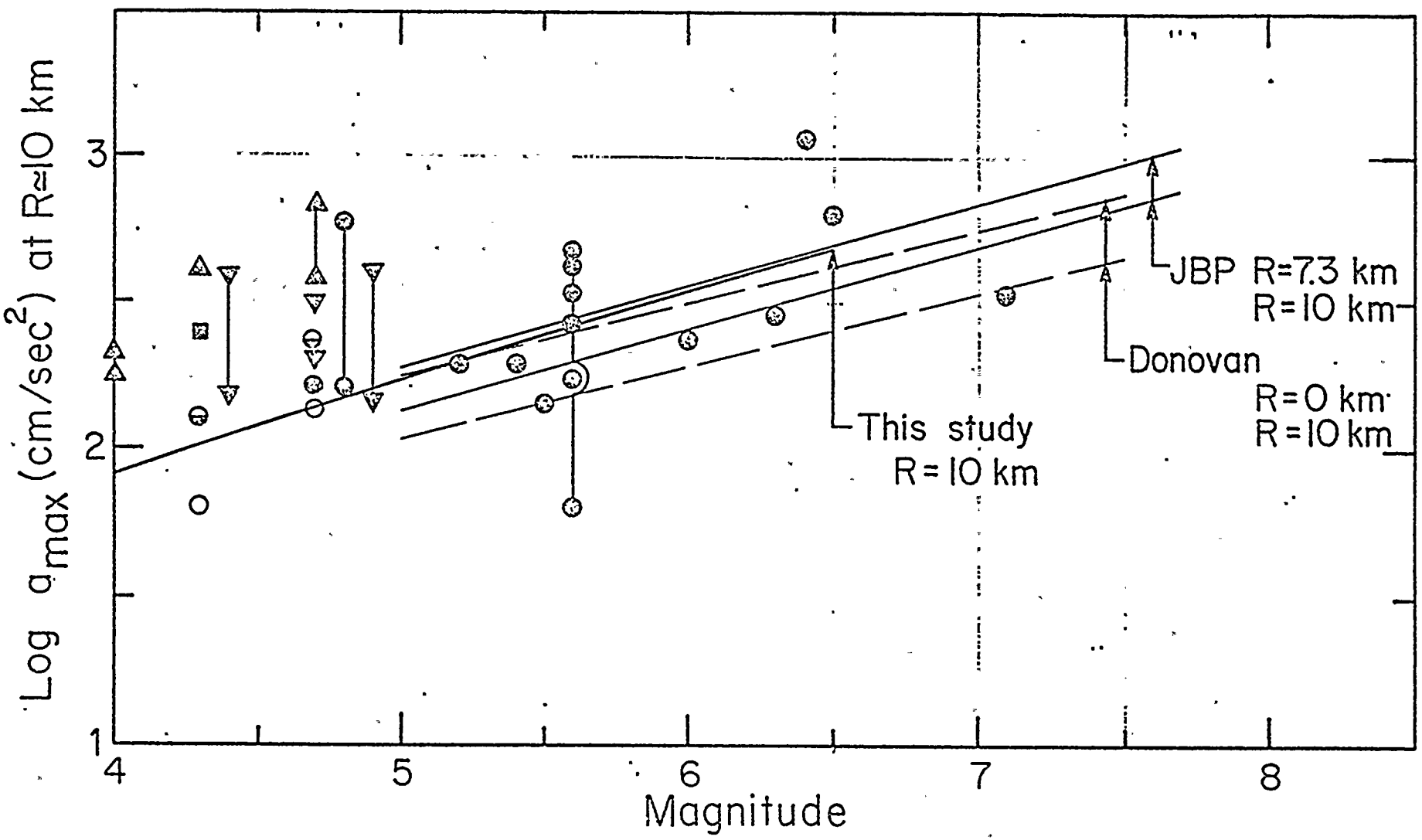
Log a_{max} (cm/sec^2) at R≈10 km
Magnitude
1
2
3
4
5
6
7
8
JBP R=7.3 km
R=10 km
Donovan
R=0 km
R=10 km
This study
R=10 km

Fig 4

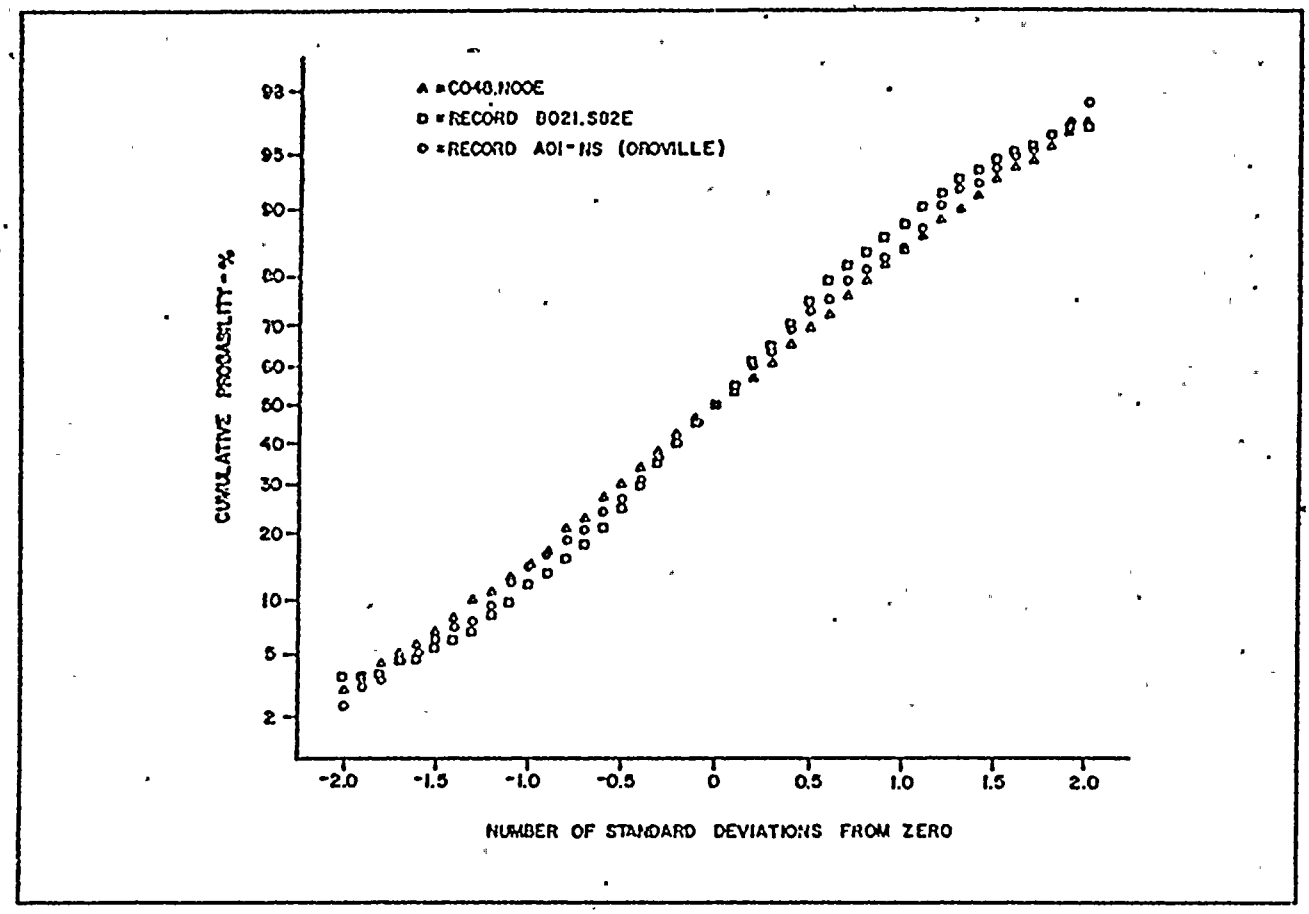
▲ = CO48.N00E
□ = RECORD B021.S02E
○ = RECORD A01-NS (OROVILLE)
CUMULATIVE PROBABILITY - %
93
95
90
80
70
60
50
40
30
20
10
5
2
-2.0
-1.5
-1.0
-0.5
0
0.5
1.0
1.5
2.0
NUMBER OF STANDARD DEVIATIONS FROM ZERO

(a)

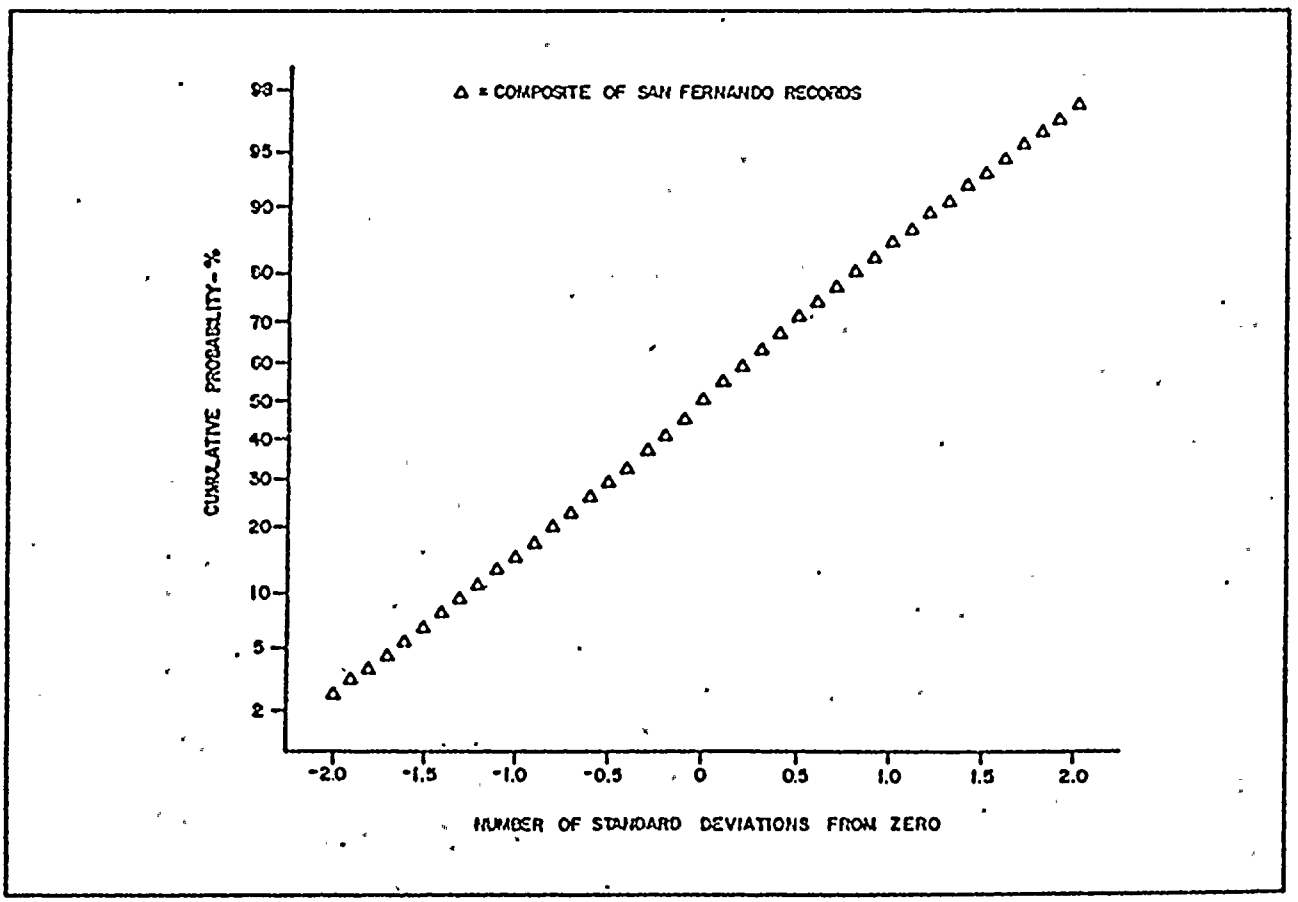
△ = COMPOSITE OF SAN FERNANDO RECORDS
CUMULATIVE PROBABILITY - %
93
95
90
80
70
60
50
40
30
20
10
5
2
-2.0
-1.5
-1.0
-0.5
0
0.5
1.0
1.5
2.0
NUMBER OF STANDARD DEVIATIONS FROM ZERO

(b)

Fig 8

Brune

SCALING LAWS FOR LARGE EARTHQUAKES
CONSEQUENCES FOR PHYSICAL MODELS

Christopher H. Scholz
Department of Geological Sciences and
Lamont-Doherty Geological Observatory
of Columbia University, Palisades, New York 10964

ABSTRACT

It is observed that the mean slip in large earthquakes correlates linearly with fault length L and is not related to fault width, W. If we interpret this in terms of an elastic model, it implies that static stress drop increases with aspect ratio (L/W). We also observe a tendency, particularly for strike-slip earthquakes, for aspect ratio, and hence static stress drop, to increase with seismic moment. Dynamic models of rupture of a rectangular fault in an elastic medium show that the final slip should be controlled by the fault width and scale with the dynamic stress drop. The only way these models can be reconciled with the observations is if dynamic stress drop correlates with fault length so that it is also nearly proportional to aspect ratio. This could only happen if fault length is determined by the dynamic stress drop. There are several serious objections to this, which lead us to suspect that these models may be poor representations of large earthquakes. Firstly, it conflicts with the observations for small earthquakes (modeled as circular sources) that stress drop is nearly constant and independent of source radius. Secondly,

it conflicts with the observation that fault length is often determined by rupture zones of previous earthquakes or tectonic complications. We speculate that the boundary condition at the base of the fault, that slip is zero, is unrealistic because that edge is in a ductile region at the base of the seismogenic layer. In a model in which slip is not so constrained at the base of the fault nor at the top (the free surface), such that no healing wave originates from these edges, final slip would be determined by fault length. The observations would then be interpreted as meaning that the static and dynamic stress drops of large earthquakes are nearly constant. These two alternatives predict very different scaling of the dynamics of large earthquakes. The width-dependent model predicts that average particle velocities are larger for long ruptures but the rise time will be the same as in a shorter event of the same width. The length-dependent model predicts the opposite.

INTRODUCTION

A central problem in earthquake seismology has been to find scaling laws that relate the static parameters such as slip and stress drop to the dimensions of the rupture and to understand these relationships in terms of the dynamic parameters, the most fundamental of which are rupture velocity and dynamic stress drop.

In doing so, it is essential to distinguish between small earthquakes and large earthquakes. Tectonic earthquakes nucleate and are bounded within a region of the earth between the surface and a depth h_o, the seismogenic layer. The seismogenic depth, h_o, depends on the tectonic environment but in a given region the maximum width of an earthquake occurring on a fault of dip δ is $W_o = h_o/\sin\delta$. We will define a small earthquake as one with a source radius $r \leq W_o/2$ and a large earthquake as one in which $r > W_o/2$. Thus a small earthquake can be represented as a circular source in an elastic medium, whereas a large earthquake is more suitably treated as a rectangular rupture with one edge at the free surface.

It has been repeatedly demonstrated (e.g., Aki, 1972; Thatcher and Hanks, 1973; Hanks, 1977) that the stress drops of small earthquakes are nearly constant and independent of source dimensions. This result, when interpreted with dynamic models of finite circular ruptures (Madariaga, 1976; Archuleta, 1976; Das, 1980), simply means that the dynamic stress drop is constant.

If the same were true for large earthquakes, the dynamic models of rectangular faulting in an elastic medium (Day, 1979; Archuleta and Day,

1980; Das, 1981) would predict that the mean slip is a linear function of fault width. In the next section we will show that this prediction is not borne out by the observations. What is observed instead is that slip correlates linearly with fault length. The principal point of this paper is to discuss the consequences of that observation for the physics of large earthquakes.

OBSERVATIONS

For small earthquakes, using the definition of seismic moment, M_o, and the relationship

$$\Delta\sigma = \frac{7\pi}{16}\mu\frac{\bar{u}}{r}$$

where r is source radius, $\bar{u}$ is mean slip, and $\Delta\sigma$ is stress drop. If stress drop is constant, the relationship between M_o and fault area, A, is

$$M_o = \left(\frac{16\Delta\sigma}{7\pi^{3/2}}\right) A^{3/2} \quad . \tag{1}$$

Large earthquakes, however, are more nearly rectangular ruptures of width W and length L and in this case, for an elastic model in which slip is restricted to be within W,

$$\Delta\sigma = C\mu\frac{\bar{u}}{W} \tag{2}$$

where C is a geometrical constant.

If stress drop were constant, we would expect to find that

$$M_o = \frac{\Delta\sigma}{C}LW^2 \tag{3}$$

In Figure 1 we show a plot of log LW^2 *vs.* log M_o, for the large interplate thrust and strike-slip earthquakes from the data set of Sykes

and Quittmeyer (1981). These observations are listed in Table 1. The data for each type of earthquake define a line, but with a slope less than one, indicating that stress drop systematically increases with moment. The offset between the data for the strike-slip and thrust events is also an important feature that we will discuss later.

These data indicate that $\bar{u}$ is not simply related to W and that $\Delta\sigma$ is not constant for large earthquakes. On the contrary, many workers (e.g., Bonilla and Buchanan, 1970; Slemmons, 1977) have argued that $\bar{u}$ correlates with L, and recently Sykes and Quittmeyer (1981) have argued that the correlation is linear. Plots of $\bar{u}$ vs. L on linear scales are shown in Figures 2 and 3 for strike-slip and thrust earthquakes, respectively.

In view of the usual uncertainties in the estimates of $\bar{u}$ and L, and any naturally occurring variations in dynamic stress drop (with which slip should be expected to scale), the correlation between $\bar{u}$ and L is fairly strong. We fit it with a straight line with an intercept at the origin

$$\bar{u} = \alpha L \tag{4}$$

and find that $\alpha \simeq 2 \times 10^{-5}$ for the thrust events and 1.25×10^{-5} for the strike-slip events. At least for the strike-slip events, slip is clearly not dependent on width because the widths of all the events in Figure 2 are between 10-15 km, i.e., they are essentially the same.

From this observation we would then expect that

$$M_o = \mu\alpha L^2 W \tag{5}$$

which is confirmed in Figure 4. For reference, the line drawn through the data has a slope of one.

Since

$$L^2W \equiv A^{3/2}\left(\frac{L}{W}\right)^{\frac{1}{2}}$$

and since the aspect ratio L/W varies only by a factor of about 20 in the data-set, we would have found a good correlation between M_o and $A^{3/2}$, as did Aki (1972) and Kanamori and Anderson (1975) had we plotted log A vs. log M_o. The question is not whether M_o correlates better with L^2W than with $A^{3/2}$. The issue of concern is that Kanamori and Anderson's interpretation of their correlation as meaning that stress drop is constant is only true if L/W is constant, because from (2) and (4), we have

$$\Delta\sigma = C\mu\alpha\frac{L}{W} \quad . \tag{6}$$

That L/W is a constant is an explicitly stated assumption of Aki (1967, 1972) and Kanamori and Anderson (1975), and although Abe (1975) and Geller (1976) attempted to observationally justify this assumption, it is not generally true. In Figures 5 and 6 we plot $\Delta\sigma$ vs. L/W for the two types of earthquakes. The correlation between them is very clear for the strike-slip events, and less so for the thrust events, for which there is a much smaller variation of aspect ratio. That L/W does not have a large variation for the thrust events seems to simply result from the fact that the seismogenic width of subduction zones, W_o, is about 100 km, so that only extremely large events can achieve high values of aspect ratio.

We can now understand why stress drop increases systematically with M_o, as shown in Figure 1. The width of large strike-slip earthquakes is

limited by the seismogenic depth to $W_o \simeq 15$ km so that they grow principally in the L direction. This results in a systematic increase in L/W, and hence $\Delta\sigma$, with M_o. The subduction zone thrust earthquakes have different widths but L increases faster than W with increasing moment, producing the same result, i.e., $\Delta\sigma$ increases with L/W or M_o. The offset between the data for thrust and strike-slip events in Figure 1 occurs simply because the widths of the thrust events are much greater than those of the strike-slip events. A strike-slip event must have a much greater aspect ratio, and hence stress drop, than a thrust event of the same moment.

PHYSICAL CONSEQUENCES

The principal feature of the observations that we wish to explain is the correlation between slip and fault length. It is a surprising observation because intuition would first lead one to expect slip to depend on width, yet this is not observed. This intuition is re-inforced by the results of dynamic models of rectangular faults in an elastic medium (Day, 1979; Archuleta and Day, 1980; Das, 1981). These models show that slip is controlled by the width of the fault and that it scales with dynamic stress drop.

The situation is illustrated in Figure 7, which shows surface slip along the fault for two representative strike-slip earthquakes. These earthquakes have essentially the same width, and differ only in length. If the dynamic stress drop were the same for these two earthquakes, then according to the theory, the Ft. Tejon earthquake would be the equivalent of six Mudurnu earthquakes placed end to end. Clearly that is not the case.

If the dynamic, elastic models are correct representations of earthquakes, then the only way they can be reconciled with the observations is if dynamic stress drop correlates with aspect ratio. Since the width of strike-slip events is nearly constant, and the width varies much less than length for the thrust events, this would be approximately true if dynamic stress drop correlates linearly with fault length. The only way this can happen without violating causality is if fault length is determined by dynamic stress drop. This is not an entirely unphysical proposition, because dynamic stress drop determines the stress intensity factor, which

is important in fracture growth. It is not obviously apparent, however, why L should increase linearly with $\Delta\sigma_d$, the dynamic stress drop.

There are several major objections to this interpretation. The first is that we have to assume that for large earthquakes $\Delta\sigma_d$ determines the rupture length, which directly contradicts the observations for small earthquakes. Although stress drop appears to increase with source radius over a limited range in some data sets (Aki, 1980), it shows no obvious variation with source radius over a very broad range (Hanks, 1977). We can offer no reasonable explanation for why large earthquakes should behave differently than small earthquakes in this important respect.

A second objection is that this assumption conflicts with the principal observations that led to the concept of seismic gaps: that the length of large earthquakes is often controlled by the rupture zones of previous earthquakes or by structural features transverse to the fault zone. Of course, one could soften the original assumption to: $\Delta\sigma_d$ determines the length unless the rupture encounters a rupture zone of a previous earthquake or a transverse feature. The rejoinder is that if the latter were as common as is thought, it would have the effect of destroying the correlation between $\bar{u}$ and L that is observed.

It is worth giving a specific example. If we compare the 1966 Parkfield earthquake (L = 30 km, $\bar{u}$ = 30 cm, W = 15 km) and the 1906 San Francisco earthquake (L = 450 km, $\bar{u}$ = 450 cm, W = 10 km) we need to explain the difference in $\bar{u}$ by a difference in $\Delta\sigma_d$ of about a factor of 15. Since the correlation between $\bar{u}$ and L is also good in these examples, we also need to argue that $\Delta\sigma_d$ determined L in these cases. On the other hand, it can be argued that the length of the 1966 earthquake was determined by the length of the gap between the rupture zone of the 1857 earthquake (or the

fault offset near Cholame) and the southern end of the creeping section of the San Andreas fault. Similarly, the 1906 earthquake filled the gap between the northern end of the creeping section at San Juan Bautista and the end of the fault at Cape Mendocino. If our argument that $\Delta\sigma_d$ determines L is true, then these latter observations are coincidences. Almost identical arguments can be made for many of the other earthquakes in our data set.

The third point is less an objection than a surprising consequence of this interpretation. The Hoei earthquake of 1707 ruptured about 500 km of the Nankai trough in Japan (Ando, 1975; Shimazaki and Nakata, 1980). The same plate boundary was ruptured twice subsequently, in two sets of delayed multiple events, the Ansei I and II events of 1854, and the Tonankai and Nankaido events of 1944 and 1946. In support of a time-predictable model of earthquake recurrence, Shimazaki and Nakata argued that the greater recurrence time between the first two sequences (147 years) and the second (91 years) is because the slip (and stress drop) were greater in 1707 than in either 1854 or 1946, the greater uplift at Muroto Point in 1707 (1.8 m) than in 1856 (1.2 m) or 1946 (1.15 m) being the evidence. The reason why this should happen is readily explained by the correlation between $\bar{u}$ and L. Thus the ratio of fault length of the Hoei and Ansei II earthquakes, 500 km/300 km = 1.7 can explain the ratio of uplift at Muroto Point, 1.8/1.2 = 1.5 and recurrence time, 147/91 = 1.6.

However, if this is interpreted as being due to a difference in dynamic stress drop, then one has to argue that a significant change in dynamic stress drop (50%) can occur on the same fault zone between successive earthquakes. One could argue that this could occur because the slip in one earthquake might change the relative position of asperities on the

fault. However, since the slip in an earthquake is about 10^{-5} L, this would mean that the gross frictional properties of the fault are controlled by asperities of dimensions on the order of 10^{-5} or less of the rupture dimensions. Since there will be a very large number of such small features, the average change between successive earthquakes would more likely be expected to be negligible.

In the above discussion we have created enough doubt about the applicability of the dynamic rectangular models to consider that they may be failing, in some fundamental way, to properly describe the physics of large earthquakes.

For a rupture propagating at a constant rupture velocity, v, the slip, for both circular and rectangular faults, is very close to [Day, 1979; Das, 1980, 1981]

$$u(x,y,t) = \dot{u}_o \left(t^2 - \frac{(x^2+y^2)}{v^2}\right)^{1/2} \quad \frac{(x^2+y^2)^{1/2}}{v} \leq t \leq t_h \qquad (7)$$

where x and y are measured relative to the point of rupture initiation. Equation (7) is the self-similar solution of Kostrov (1964). The asymptotic particle velocity, $\dot{u}_o$ which scales the slip is, (Kostrov, 1964; Dahlen, 1974)

$$\dot{u}_o = K\frac{\Delta\sigma_d}{\mu}\beta \qquad (8)$$

where K is a function of rupture velocity.

When the rupture reaches its final perimeter and stops, a healing wave propagates back into the rupture, arriving at time t_h. For $t > t_h$ slip decelerates and comes to a halt. The healing wave is not the stopping phase, which is a wave radiated in all directions from the tip of a

stopping crack (Savage, 1965). A stopping phase cannot physically stop the slip in these models because such a wave will lose energy with distance whereas the results of the models are independent of dimension. A healing wave must be interpreted as a wave that propagates into the interior of the rupture in an analogous way, and for analogous physical reasons, as the stopping of cars on a highway propagates up the stream of traffic. Causality restricts it to travel at a velocity slower than a stopping phase. Thus Madariaga (1976, p. 648) observed, "It appears as if a 'healing' wave propagates inward from the edge of the fault some time after the P and S stopping phases."

Since slip is terminated by the healing wave, the rise time and final slip at any point on the fault is determined by the distance to the nearest boundary (Day, 1979; Das, 1981). Therefore it is easy to see why mean slip on a rectangular fault should be controlled by the fault width.

A healing wave is the result of the boundary condition that $u = 0$ at the edges of the fault. If the models are poor representations of large earthquakes, the most likely problem is that these boundary conditions are unrealistic. The models are of rectangular faults embedded in an elastic whole space. The boundary condition $u = 0$ is imposed on all edges of the fault and healing waves thus propagate from each edge. Since large earthquakes rupture the free surface, slip is unconstrained there and a healing wave will not propagate from that edge. However even if an elastic half-space model were available, we would still expect slip to be width-dependent since it would be controlled by the healing wave from the base of the fault.

In large earthquakes the base of the fault is at the bottom of the seismogenic layer. A plausible explanation for the seismogenic depth is

that it is the result of a brittle-ductile transition. Thus a large earthquake cannot propagate to greater depth because the energy at the crack tip is dissipated in plastic deformation. A more realistic model then may be one in which the base of the fault is in a plastic, rather than elastic, region and therefore the condition $u = 0$ is no longer valid at that edge.

We illustrate in Figure 8 the difference between an elastic model and an elastic-plastic model. The most significant difference is that in the elastic-plastic model (Figure 8b) slip at the base of the fault may be allowed to be greater than zero as a result of plastic deformation in a zone surrounding the rupture tip. This is simply the equivalent, in shear, of the blunting of a crack tip that occurs in tensile crack propagation in ductile materials. The plastic deformation around the base of the fault smooths out the stress singularity associated with finite slip there, and will continue as long as slip continues. This may have the effect of inhibiting a healing wave from originating at the base, and if healing waves propagate only from the ends of the fault, slip and rise time will depend on fault length, not width.

No model is available with these boundary conditions but we can approximate one. If we make the approximation that slip stops abruptly with the arrival of the healing wave, then the final slip on the fault will be, from (7),

$$u(x,y) = \dot{u}_o\left(t_h^2 - \frac{(x^2+y^2)}{v^2}\right)^{1/2} \qquad (9)$$

which we can calculate. This is a 'quasidynamic' model (Boatwright, 1980), i.e., a kinematic model that simulates a dynamic model.

It can readily be shown for the circular case that (9) yields final slip values that are everywhere within 5% of that of the dynamic numerical models of Madariaga (1976) and Das (1980), and Day (1979) has shown that (9), when properly truncated, also yields a very good approximation to final slip in his rectangular models. We use it to simulate an elastic-plastic half-space model by simply assuming that no healing wave propagates from either the top or bottom of the fault.

The procedure we use is very similar to that used by Day (1979, pp. 23-26), and simply involves the calculation of t_h. We assumed $v = 0.9\beta$, for which the corresponding value of K is 0.81 (Dahlen, 1974), and that the velocity of the healing wave is $\sqrt{3}\beta$. In Figure 9 we show slip at the surface as a function of distance from the center of the fault for a bilateral case with L/W = 4. The mean slip is found to scale as

$$\bar{u} = \frac{1}{2}\frac{\Delta\sigma_d}{\mu}L \qquad (10)$$

so this model would lead to the interpretation that the linear correlation between $\bar{u}$ and L that is observed means that the dynamic stress drop for large interplate earthquakes is approximately constant. Equating (10) with (4) we obtain $\Delta\sigma_d \simeq 12$ bars and 7.5 bars for thrust and strike-slip earthquakes, respectively. Returning to Figure 4, the line drawn through the data is the prediction of this model for $\Delta\sigma_d = 10$ bars. Furthermore, in this model, where slip is unconstrained at top and bottom, static stress drop will also be a function of fault length, since the scale length that determines the strain change will be the fault length. The observation made earlier that $\Delta\sigma$ is a function of aspect ratio is due to the incorrect use of equation (2) to calculate it. According to this model, $\Delta\sigma$ is also approximately constant for these earthquakes.

DISCUSSION

The observation that slip increases with fault length in large earthquakes poses severe consequences when viewed in the light of dynamic rupture models. In conventional dynamic models (W models), slip is determined by fault width, rather than length. These models can only be reconciled with the observations if it is assumed that the dynamic stress drop determines the fault length, and the several major objections to this possibility were detailed earlier. With different assumptions concerning the boundary conditions at the base of the fault, it may be possible to construct a dynamic model in which slip depends on fault length (L model). This model avoids the objections raised to the W model but is based on a speculative, although not entirely ad hoc, assumption concerning the boundary conditions.

Furthermore, severe constraints are placed on L models from the geodetic data obtained for the 1906 San Francisco earthquake. The simplest form of L model is one in which slip is totally unconstrained at the base of the fault. If this were the case, strain release would extend out to distances comparable to fault length, rather than depth, but as Brune (1974) has pointed out, the strain release in 1906 was concentrated within a few tens of km from the fault. From angle changes in the Pt. Arena triangulation network [angle † from Thatcher (1975, Fig. 4)] one can estimate a strain drop of 8×10^{-5} within 12 km of the fault, a figure somewhat more consistent with a W model than an L model. Thus if L models are relevant, they must be models in which slip is only <u>partially</u> constrained at the base of the fault. In the absence of numerical modeling of

this type, one can't tell if this type of model will result in L scaling or hybrid scaling intermediate to the L and W extremes.

These L and W models represent, in many respects, opposite extremes concerning the mechanism of large earthquakes and so it is useful to discuss the contrasting way in which they scale. For earthquakes in which $L < 2W$, the models are indistinguishable in their gross manifestations. In Figure 10 we schematically show a comparison between an earthquake of dimensions about $L = 2W$ and one of the same width but about 15 times longer. Specifically, this might be a comparison of the 1966 Parkfield earthquake, say, and the 1906 San Francisco earthquake.

On the left of the figure we show a snapshot of slip on the fault during the smaller earthquake. We only show the part that is actually slipping during the snapshot. We also show the time history of slip at some representative point. For simplicity, it is simply shown as a ramp with a rise time, t_R. On the right is shown the predictions of the two models for the longer earthquake.

In a bilateral case, as shown, the W model predicts that the slipping portion of the fault splits into two patches of length $\sim W$ that propagate away from each other at a velocity $2v$ as they sweep over the fault surface. Since the rise time $t_R \simeq W/2\beta$, remains the same but the slip is fifteen times greater, the dynamic stress drop, and hence particle velocity, must be fifteen times greater.

In the L model, the rupture sweeps out over the fault as an expanding patch, with slip continuing within its boundaries until after the final dimensions are reached. In that model, the dynamic stress drop and particle velocities are the same as in the smaller event, but the rise time, $t_R \simeq L/2\beta$ is much longer.

In terms of predicting the strong ground motions for a 1906 size earthquake, say, from observed ground motions for a 1966 size earthquake, the difference between the W and L model is critical. The W model would predict that the average particle velocities would be much higher and the duration would be about the same. The L model would predict nearly the opposite.

Suppose we start with a square rupture of width W_o and consider how peak particle velocity, $\dot{u}_p$, and the asymptotic particle velocity, $\dot{u}_o$, increase for ruptures of greater length. For a square rupture with dynamic stress drop, $\Delta\sigma_d^S$, the maximum value of $\dot{u}_p$ and the asymptotic value $\dot{u}_o$ will be

$$\dot{u}_p^S \propto \Delta\sigma_d^S \sqrt{W_o}$$

and (11)

$$\dot{u}_o^S \propto \Delta\sigma_d^S$$

Using the W model, for a rupture of width W_o and length $L > W_o$, the stress drop will have to be greater by the ratio

$$\frac{\Delta\sigma_d^W}{\Delta\sigma_d^S} = \frac{L}{W_o}$$

so that

$$\dot{u}_p^W \propto \Delta\sigma_d^S \frac{L}{W_o} \sqrt{W_o}$$

and (12)

$$\dot{u}_o^W \propto \Delta\sigma_d^S \frac{L}{W_o}$$

For the L model, stress drop is the same but the scale length that determines the maximum peak velocity becomes L rather than W, so that

$$\dot{u}_p^L \propto \Delta\sigma_d^S \sqrt{L}$$

and (13)

$$\dot{u}_o^L \propto \Delta\sigma_d^S$$

Comparing (12) and (13), the two models differ in the ratios

$$\frac{\dot{u}_p^L}{\dot{u}_p^W} = \sqrt{\frac{W_o}{L}}$$

and (14)

$$\frac{\dot{u}_o^L}{\dot{u}_o^W} = \frac{W}{L}$$

So that with a W model, from (12), both peak and asymptotic velocities for a 1906 type earthquake would be about 15 times greater than for the Parkfield earthquake. For the L model, from (13), the peak velocities would at maximum be about $\sqrt{15}$ greater for a 1906 than a 1966 event, but the asymptotic value would be the same.

These remarks, of course, apply only to the simple case of a smoothly propagating rupture. Any heterogeneity will produce local high frequency variations in the velocities. However, they serve to point out the importance of determining if large earthquakes are better described by an L model or W model or by some intermediate case, if such can exist.

ACKNOWLEDGEMENTS

My attempts at trying to understand the consequences of slip correlating with fault length had a rather long gestation period, during which the author benefitted from discussions with T. Hanks, J. Boatwright, P. Richards, S. Das, S. Day, and R. Madariaga. Most of the work was done while the author was a visitor at the Department of Earth Sciences, University of Cambridge, and a Green Scholar at the Institute of Geophysics and Planetary Physics, University of California, San Diego. Both are thanked for their support and hospitality. The work was supported by National Science Foundation grant EAR 80-07426 and National Aeronautics and Space Administration grant NGR 33-008-146. I thank P. Richards and L. Sykes for critical reviews. Lamont-Doherty Geological Observatory contribution no. 0000.

REFERENCES

Abe, K. (1975). Reliable estimation of the seismic moment of large earthquakes, J. Phys. Earth, 23, 381-390.

Aki, K. (1967). Scaling law of seismic spectrum, J. Geophys. Res., 72, 1217-1231.

Aki, K. (1972). Earthquake mechanism, Tectonophysics, 13, 423-446.

Aki, K. (1980). Re-evaluation of stress drop and seismic energy using a new model of earthquake faulting, in Source Mechanism and Earthquake Prediction, p. 23-50, Edit. Centre Nat. Recherche Sci., Paris.

Ambraseys, N. (1970). Some characteristics of the Anatolian fault zone, Tectonophysics, 143-165.

Archuleta, R. J. (1976). Experimental and numerical three dimensional simulations of strike-slip earthquakes, Ph.D. thesis, Univ. of Calif., San Diego.

Archuleta, R. J., and S. M. Day (1980). Dynamic rupture in a layered medium: the 1966 Parkfield earthquake, Bull. Seismol. Soc. Amer., 20, 671-689.

Ando, M. (1975). Source mechanisms and tectonic significance of historic earthquakes along the Nankai trough, Japan, Tectonophysics, 27, 119-140.

Boatwright, J. (1980). A spectral theory for circular seismic sources; simple estimates of source dimension, dynamic stress drop, and radiated seismic energy, Bull. Seismol. Soc. Amer., 70, 1-27.

Bonilla, M. G., and J. M. Buchanan (1970). Interim report on worldwide historic surface faulting, U. S. Geol. Surv. Open-File Rept., Washington, D.C.

Brune, J. N. (1974). Current status of understanding quasi-permanent fields associated with earthquakes, EOS, Trans. AGU, 55, 820-827.

Dahlen, F. A. (1974). On the ratio of P-wave to S-wave corner frequencies for shallow earthquake sources, Bull. Seismol. Soc. Amer., 64, 1159-1180.

Das, S. (1980). A numerical method for determination of source-time functions for general three-dimensional rupture propagation, Geophys. J. R. Astron. Soc., 62, 591-604.

Das, S. (1979). Three-dimensional spontaneous rupture propagation and implications for the earthquake source mechanism, Geophys. J. R. Astron. Soc., in press.

Day, S. (1979). Three-dimensional finite difference simulation of fault dynamics, Final Rept., NAS2-10459, 71 pp., Systems, Science and Software, La Jolla, Calif.

Geller, R. J. (1976). Scaling relations for earthquake source parameters and magnitudes, Bull. Seismol. Soc. Amer., 66, 1501-1523.

Hanks, T. C. (1977). Earthquake stress drops, ambient tectonic stress, and stresses that drive plate motions, Pure Appl. Geophys., 115, 441-458.

Kanamori, H., and D. L. Anderson (1975). Theoretical basis of some empirical laws of seismology, Bull. Seismol. Soc. Am., 65, 1073-1096.

Kostrov, B. V. (1964). Selfsimilar problems of propagation of shear cracks, J. Appl. Math. Mech., 28, 1077-1087.

Madariaga, R. (1976). Dynamics of an expanding circular fault, Bull. Seismol. Soc. Amer., 66, 639-666.

Savage, J. C. (1965). The stopping phase on seismograms, Bull. Seismol. Soc. Amer., 55, 47-58.

Shimazaki, K., and T. Nakata (1980). Time-predictable recurrence model for large earthquakes, Geophys. Res. Lett., 7, 279-282.

Sieh, K. (1978). Slip along the San Andreas fault associated with the great 1857 earthquake, Bull. Seis. Soc. Amer., 68, 1421-1448.

Slemmons, D. B. (1977). State of the art for assessing earthquake hazards in the United States, Faults and earthquake magnitudes, U.S. Army Eng. Waterway Exp. Sta., Vicksburg, Miss., pp. 229, 1977.

Sykes, L. R., and R. C. Quittmeyer (1981). Repeat times of great earthquakes along simple plate boundaries, Third Maurice Ewing Symposium on Earthquake Prediction, 4, edited by D. W. Simpson and P. G. Richards, AGU, Washington, D.C.

Thatcher, W. (1975). Strain accumulation and release mechanism of the 1906 San Francisco earthquake, J. Geophys. Res., 80, 4862-4872.

Thatcher, W., and T. Hanks (1973). Source parameters of southern California earthquakes, J. Geophys. Res., 78, 8547-8576.

TABLE 1

PARAMETERS OF LARGE INTERPLATE EARTHQUAKES
(AVERAGED FROM SYKES AND QUITTMEYER (1981))

No.	Date	Location	Mo 10^{27} dyne-cm	L km	W km	L/W	$\bar{u}$ cm	$\Delta\sigma$ bars
		Strike-Slip Earthquakes						
1.	10 Jul 1958	SE Alaska	4.3	350	12	29	325	26
2.	9 Jan 1857	S. California	7	380	12	32	465	36
3.	18 Apr 1906	San Francisco	4	450	10	45	450	44
4.	19 May 1940	Imperial Va., Ca.	0.23	60	10	6	125	13
5.	27 Jun 1966	Parkfield, Calif.	0.03	37	10	4	30	4
6.	9 Apr 1968	Borrego Mtn, Ca.	0.08	37	12	3	25	3
7.	15 Oct 1979	Imperial Va., Ca.	0.03	30	10	3	30	4
8.	4 Feb 1976	Guatemala	2.6	270	15	18	150	9
9.	16 Oct 1974	Gibbs F. Z.	0.45	75	12	6	170	14
10.	26 Dec 1939	Ercincan, Turkey	4.5	350	15	23	285	18
11.	20 Dec 1942	Erbaa Niksar, Turkey	0.35	70	15	5	112	8
12.	1 Feb 1944	Gerede-Bolu, Turkey	2.4	190	15	13	275	18
13.	18 Mar 1953	Gönen-Yenice, Turkey	0.73	58	15	4	280	21
14.	22 Jul 1967	Mudurnu, Turkey	0.36	80	15	5	100	7
		Thrust Earthquakes						
15.	6 Nov 1958	Etorofu, Kuriles	44	150	70	2.1	840	37
16.	13 Oct 1963	Eruppu, Kuriles	67	275	110	2.5	445	12
17.	16 May 1968	Tokachi-oki, Japan	28	150	105	1.4	355	10
18.	11 Aug 1969	Shikotan, Kuriles	22	230	105	2.2	180	5
19.	17 Jun 1973	Nemuro-oki, Japan	6.7	90	105	0.86	140	5
20.	4 Nov 1952	Kamchatka	350	450	175	2.6	890	14
21.	28 Mar 1964	Prince Wm Sound, Alaska	820	750	180	4.2	1215	18
22.	4 Feb 1965	Rat Island, Aleutians	125	650	80	8.1	480	10
23.	10 Jan 1973	Colima, Mexico	3	85	65	1.3	110	5
24.	29 Nov 1978	Oaxaco, Mexico	3	80	70	1.1	110	5
25.	22 May 1960	S. Chile	2000	1000	210	4.8	1900	21
26.	17 Oct 1966	C. Peru	20	80	140	0.6	360	12

FIGURE CAPTIONS

Figure 1. Plot of $\log LW^2$ *vs.* $\log M_o$ for the large intraplate earthquakes from the data set of Sykes and Quittmeyer (1981). The lines of slope 1 are constant stress drop lines, assuming C = 0.6 for the thrust events, and 0.3 for the strike-slip events.

Figure 2. A plot of mean slip, $\bar{u}$, *vs.* fault length for the strike-slip events. The line drawn through the data has a slope of 1.25×10^{-5}. Numbers are references to Table 1.

Figure 3. The same as Figure 2, for the thrust events. The slope of the line is 2×10^{-5}.

Figure 4. A plot of $\log L^2W$ *vs.* $\log M_o$. The line drawn through the data has a slope of 1, for reference.

Figure 5. Stress drop plotted *vs.* aspect ratio for the strike-slip earthquakes.

Figure 6. Stress drop *vs.* aspect ratio for the thrust earthquakes. Event 22 is an oblique slip event for which stress drop was calculated based only on the dip slip component and is hence underestimated. Event 15 is an anomalously deep event in the Kuriles (Sykes and Quittmeyer, 1981).

Figure 7. Schematic representation of two models of large earthquakes. In A, it is represented by rupture in an elastic half-space. The boundary condition at the base of the rupture is $u = 0$. In B, the rupture penetrates a ductile region. At the base $u > 0$, which is accommodated by plastic deformation in a zone surrounding the rupture tip.

Figure 8. Surface slip as a function of distance along the fault plane for two representative strike-slip earthquakes of similar width but different depth. Data for the Mudurnu earthquake is from Ambraseys (1969) and for the Ft. Tejon earthquake from Sieh (1978).

Figure 9. Dimensionless slip, u' vs. length, L', at the free surface from the center to the end of the fault. The model is a quasidynamic one that simulates a dynamic model with boundary conditions similar to those shown in Figure 7b, as described in the text. The normalization relations are $u = \frac{\Delta\sigma_d}{\mu} W u'$ and $L = WL'$. The case shown is bilateral with aspect ratio 4.

Figure 10. A schematic diagram to illustrate the contrasting way in which a model in which width determines the slip (W model) scales with length as compared to a length dependent model (L model).

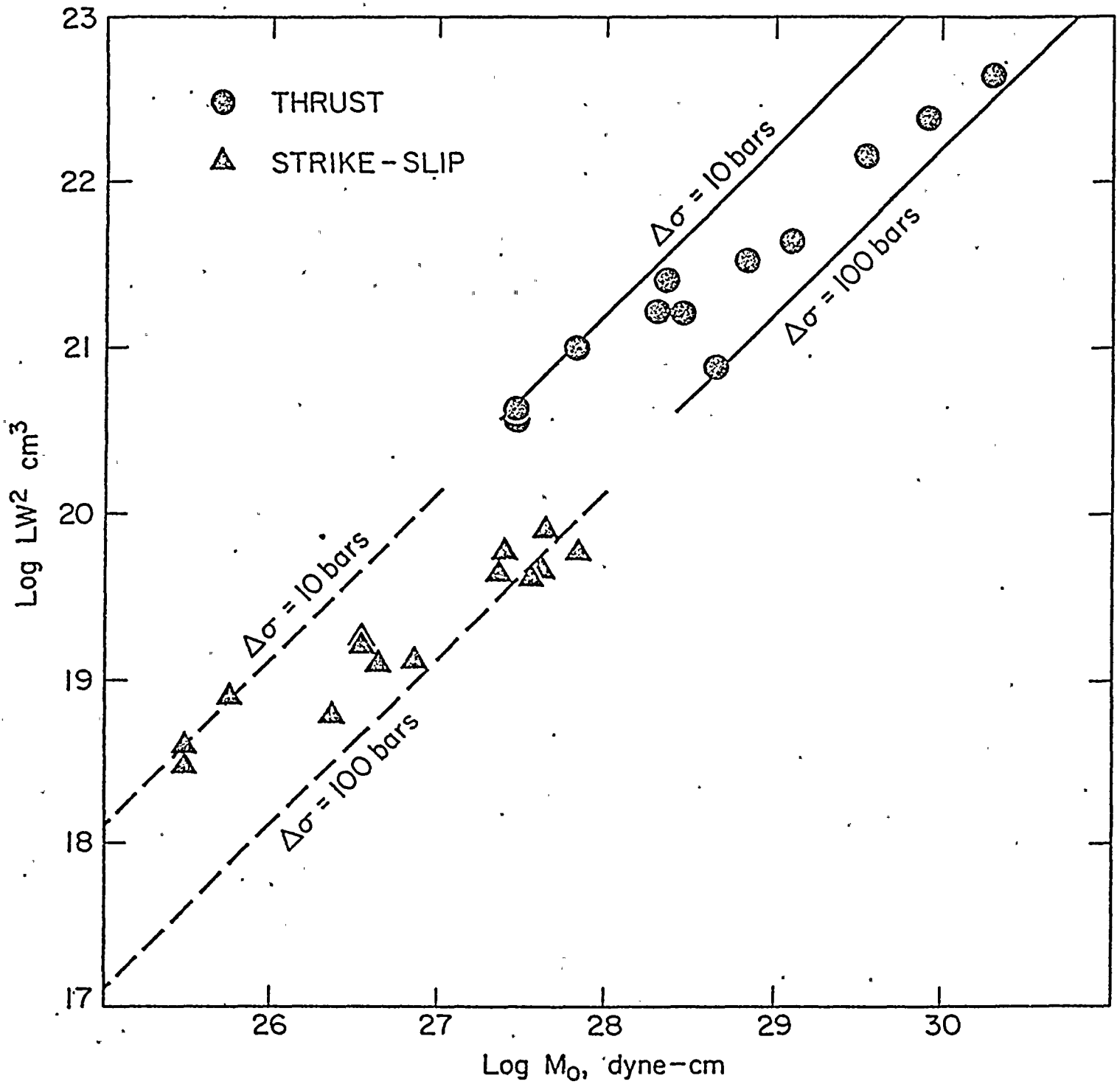
THRUST
STRIKE-SLIP
Δσ = 10 bars
Δσ = 100 bars
Δσ = 10 bars
Δσ = 100 bars
Log LW² cm³
Log M₀, dyne-cm
23
22
21
20
19
18
17
26
27
28
29
30

Figure 1

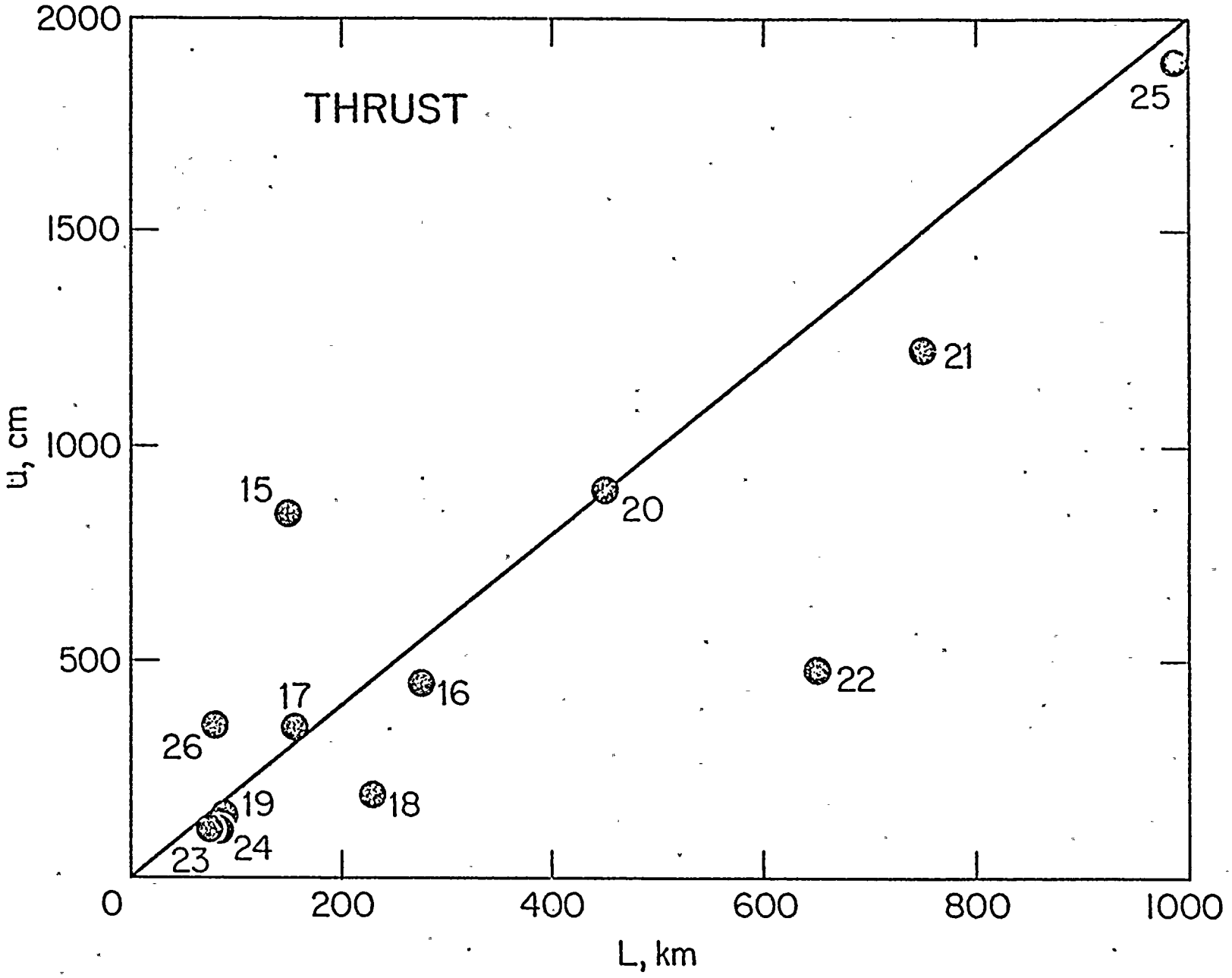
THRUST
2000
1500
1000
500
0
200
400
600
800
1000
u, cm
L, km
25
21
15
20
17
16
22
26
19
18
24
23

Figure 3

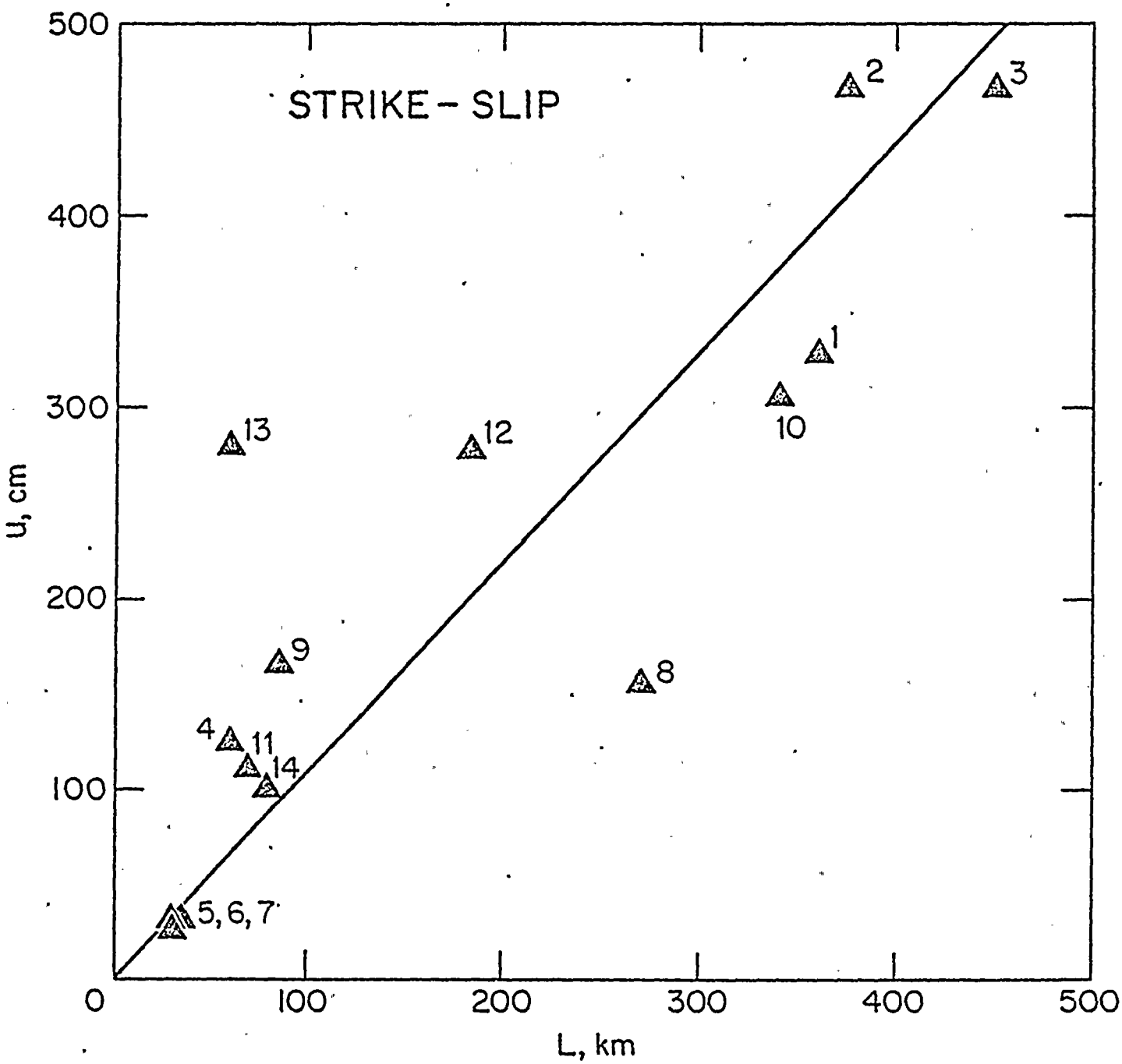
STRIKE – SLIP
500
400
300
200
100
0
100
200
300
400
500
u, cm
L, km
1
2
3
4
5, 6, 7
8
9
10
11
12
13
14

Figure 2

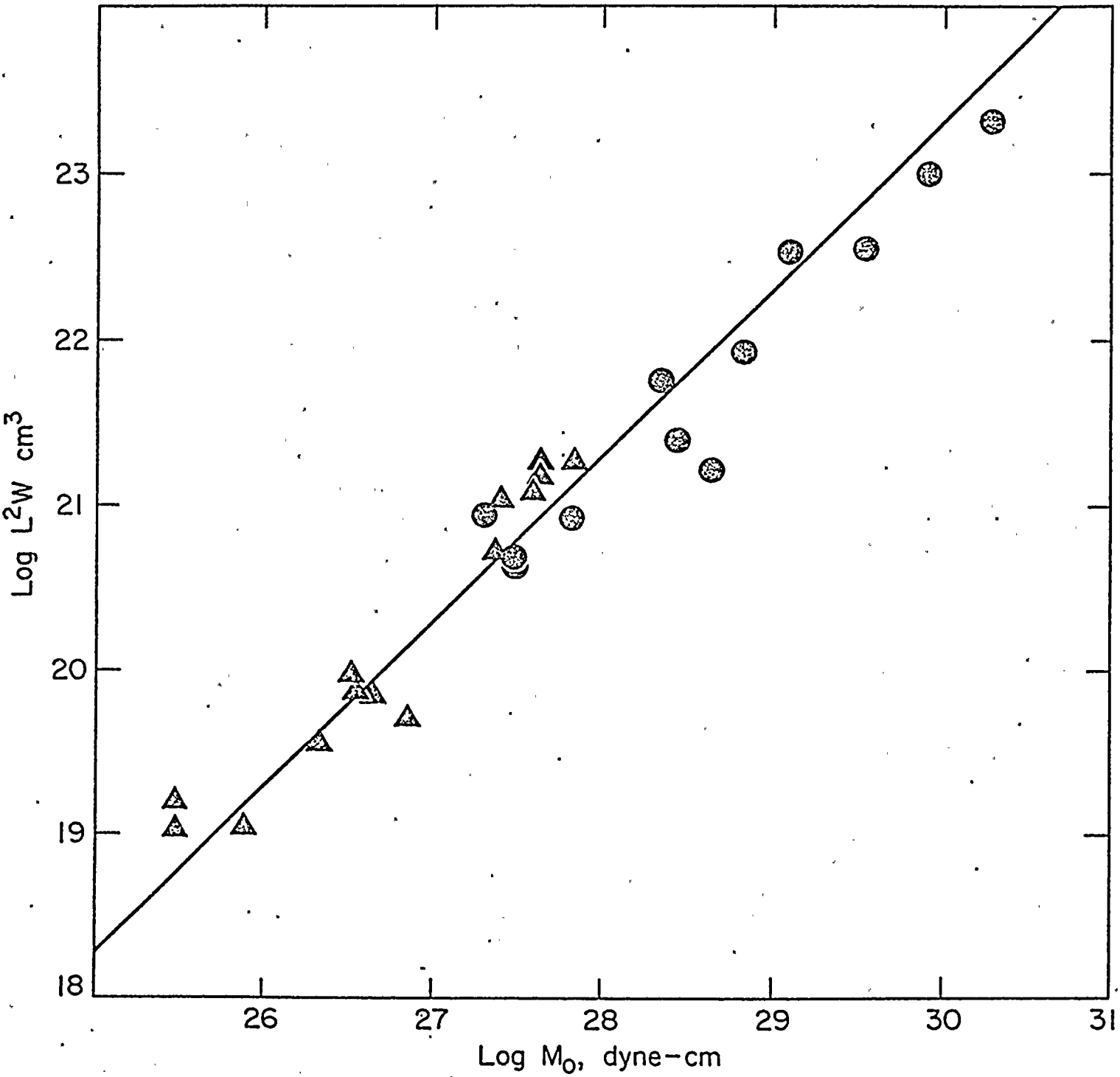

Figure 4

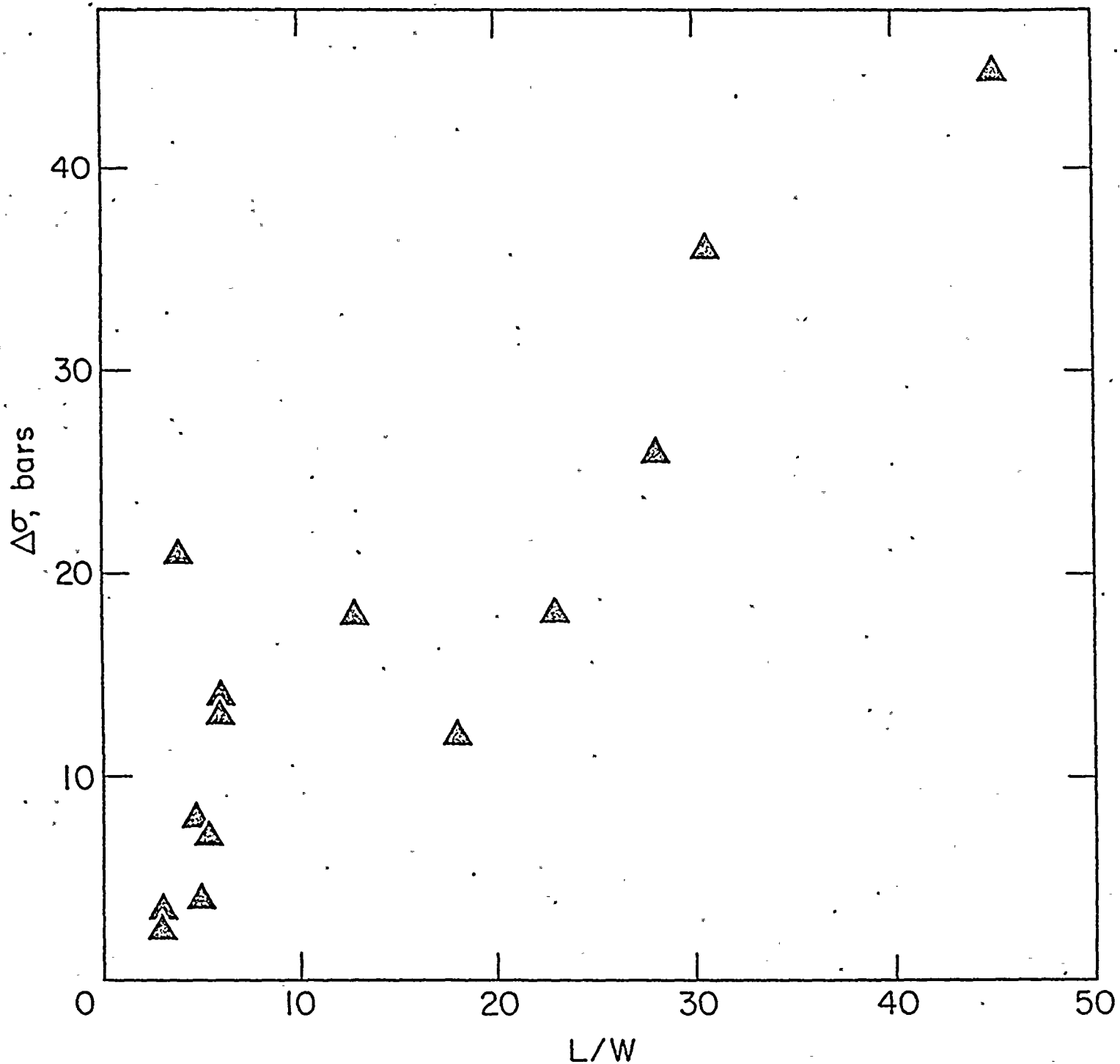

Figure 5

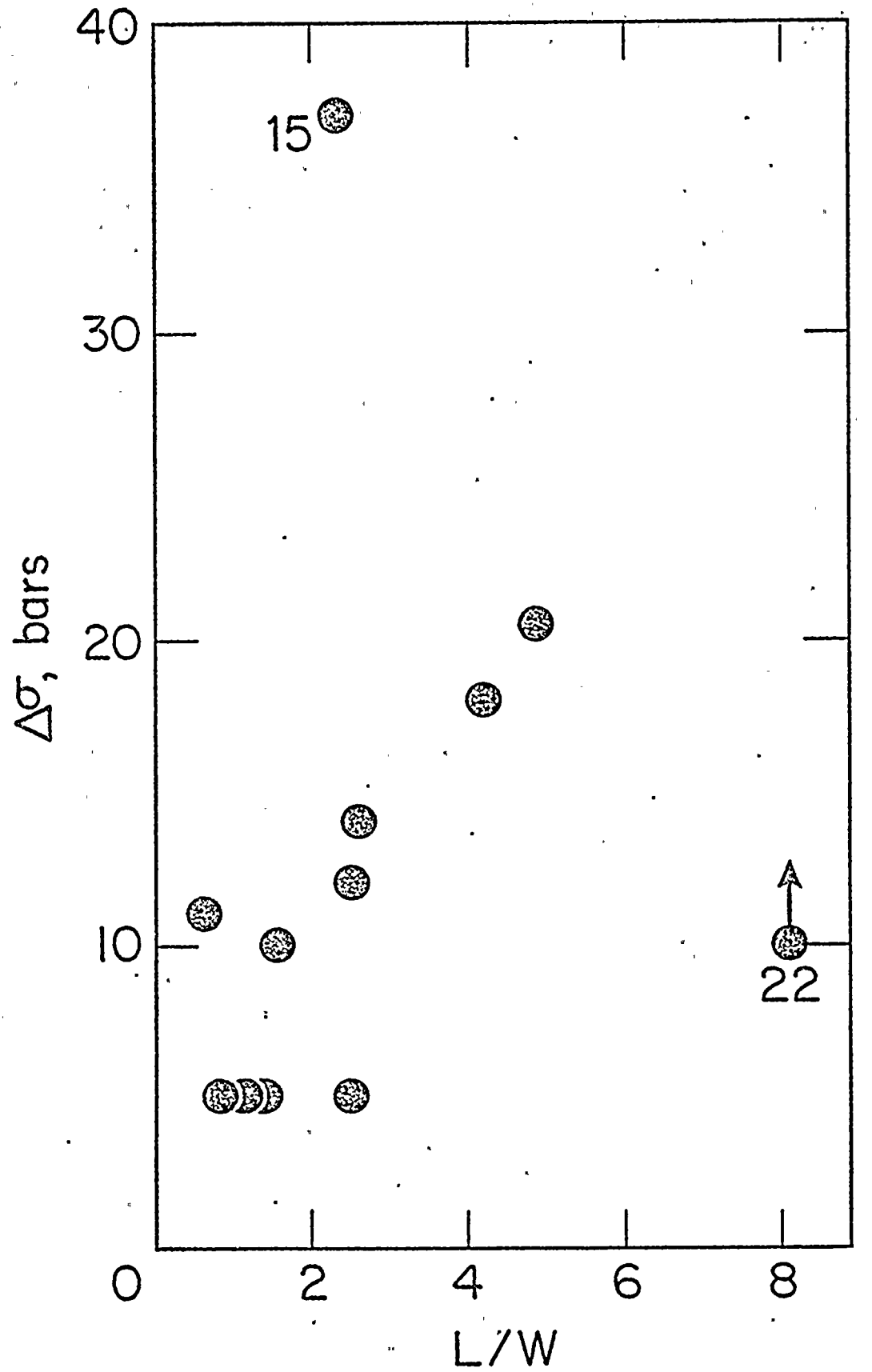

Figure 6

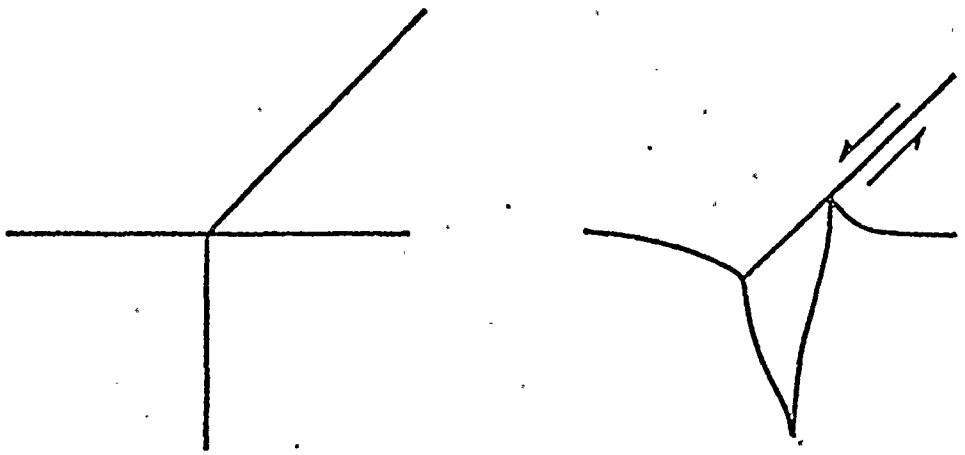

A

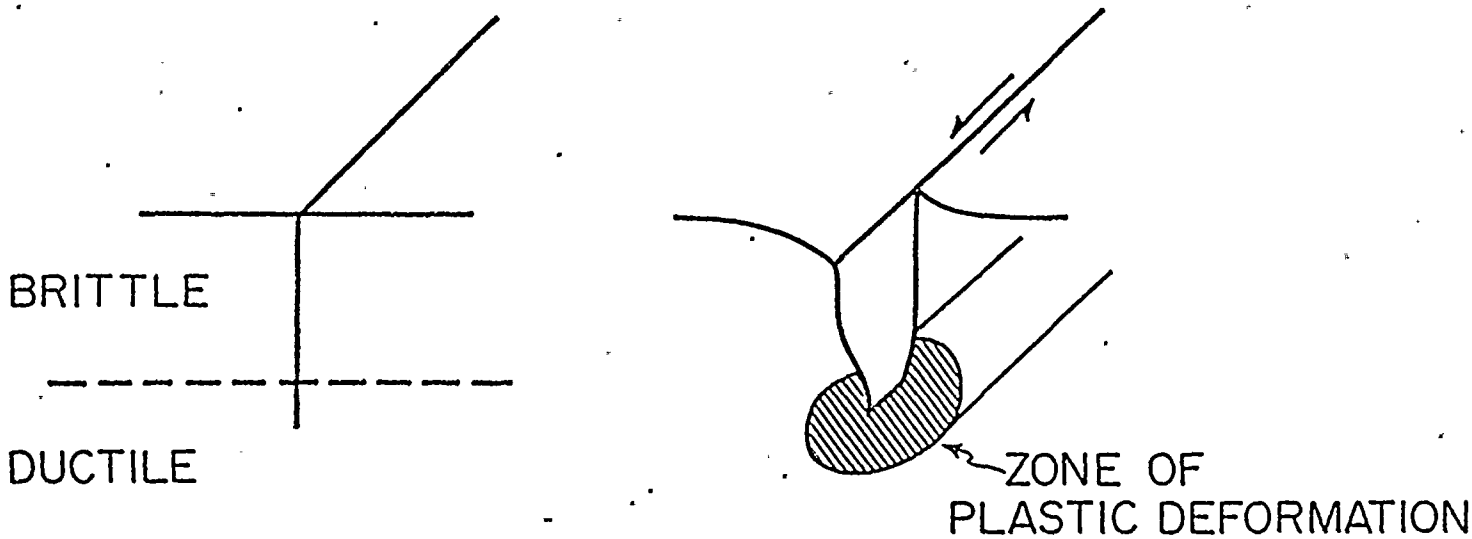

B

Figure 7

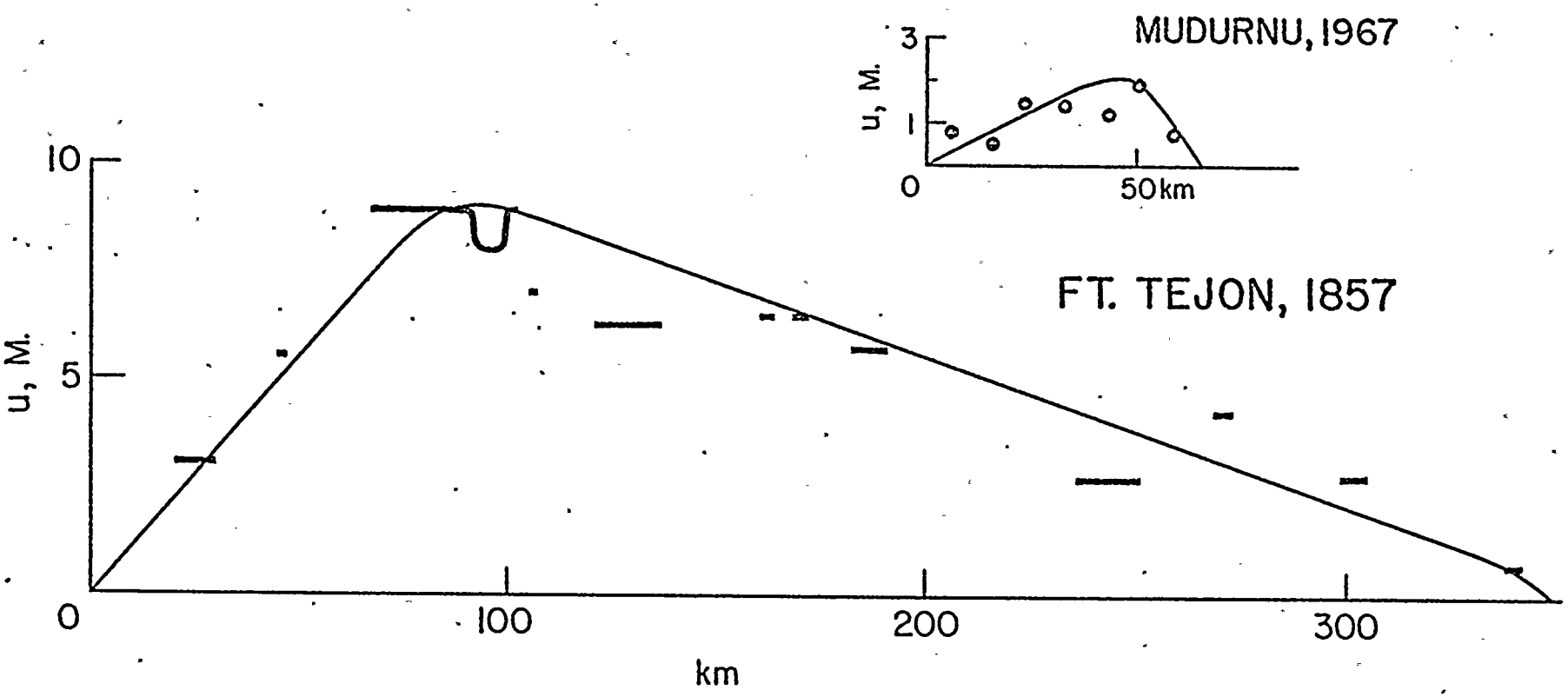

Figure 8

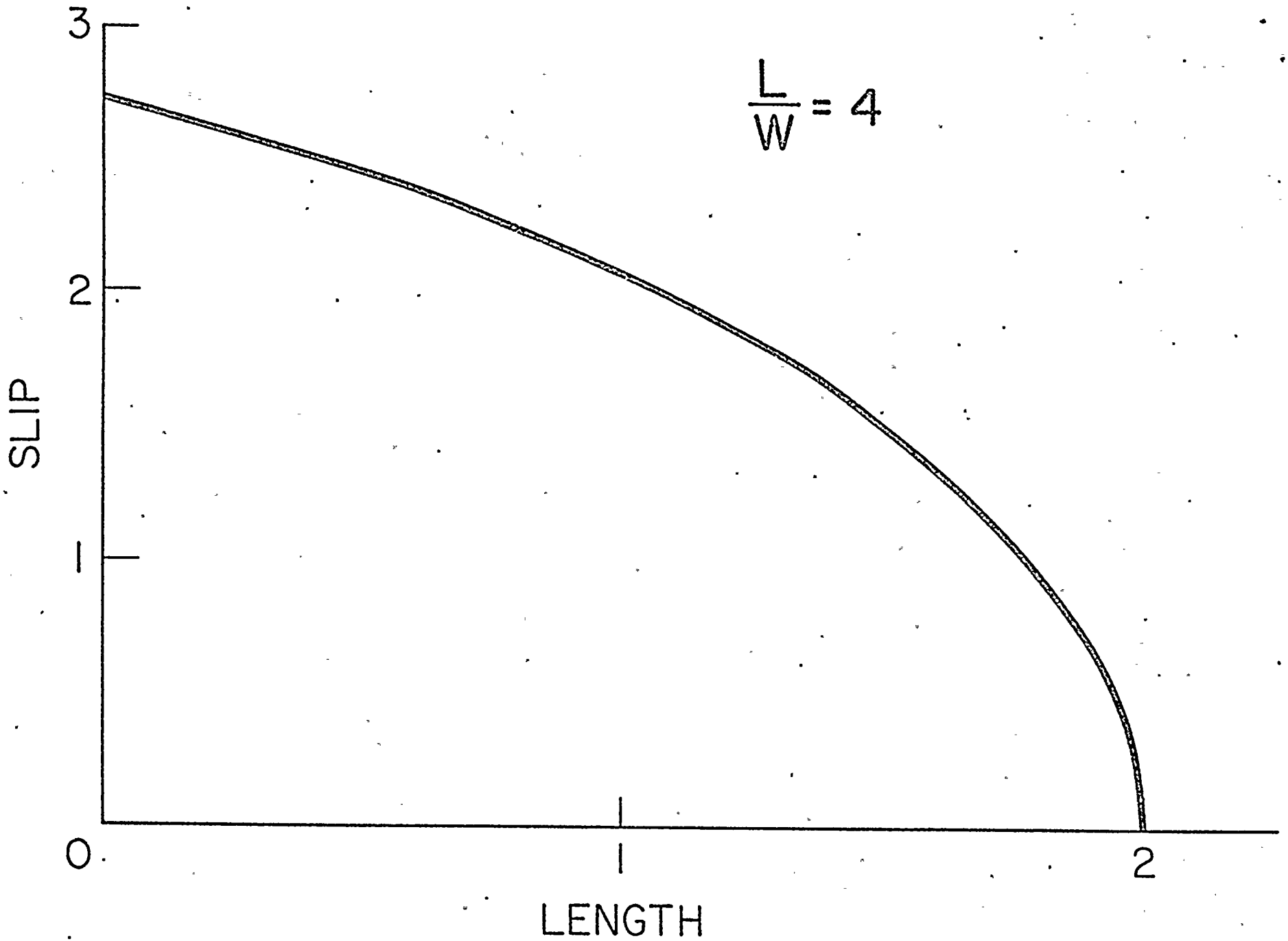

Figure 9

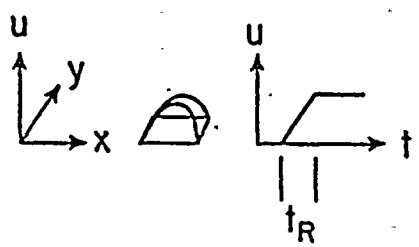

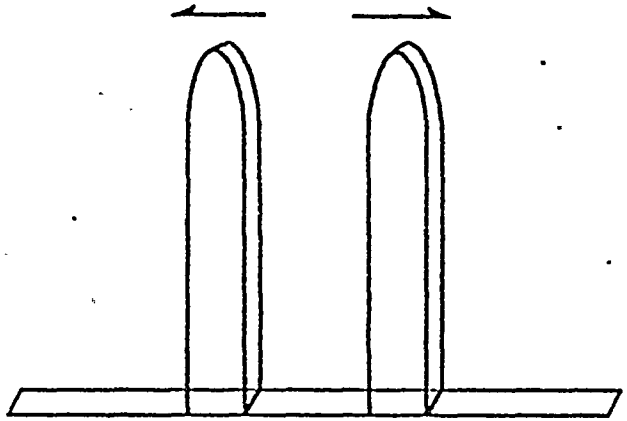

W - MODEL

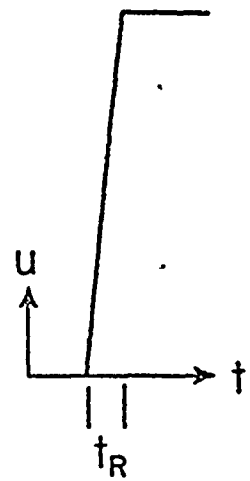

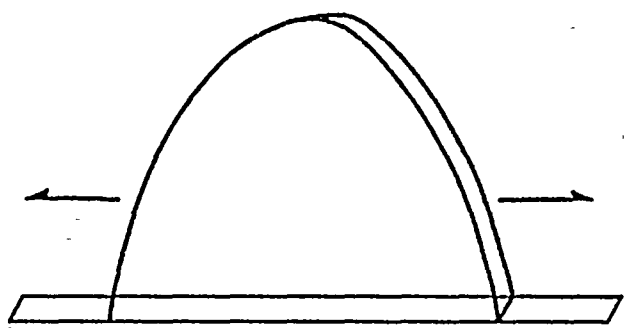

L - MODEL

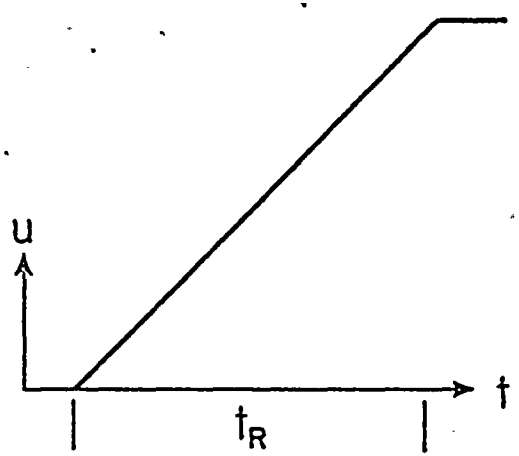

Figure 10

UNITED STATES OF AMERICA
NUCLEAR REGULATORY COMMISSION

BEFORE THE ATOMIC SAFETY AND LICENSING APPEAL BOARD

In the Matter of:	)	
PACIFIC GAS & ELECTRIC COMPANY (Diablo Canyon Nuclear Power Plant, Units 1 & 2	)	Docket Nos. 50-275 O.L. 50-323 O.L.

CERTIFICATE OF SERVICE

I hereby certify that on this 24th day of May, 1981 I have served copies of the foregoing MOTION TO REOPEN THE RECORD by mailing them through the U.S. Mail, first-class, postage pre-paid, to those persons listed below, except those designated by an asterisk on whom service was made by messenger on May 26, 1981.

* Richard S. Salzman, Chairman
Atomic Safety & Licensing Appeal Board
U.S. Nuclear Regulatory Commission
4350 East West Highway
Bethesda, Maryland 20014

* Dr. W. Reed Johnson
Atomic Safety & Licensing Appeal Board
U.S. Nuclear Regulatory Commission
4350 East West Highway
Bethesda, Maryland 20014

* Dr. John H. Buck
Atomic Safety & Licensing Appeal Board
U.S. Nuclear Regulatory Commission
4350 East West Highway
Bethesda, Maryland 20014

John F. Wolf
Chairman
Atomic Safety & Licensing Board
3409 Shepherd Street
Chevy Chase, Maryland 20015

Docket & Service Section
Office of the Secretary
U.S. Nuclear Regulatory
Commission
Washington, D.C. 20555

William J. Olmstead, Esq.
Edward G. Ketchen, Esq.
Lucinda Low Swartz
Charles A. Barth
Office of the Executive Legal
Director - BETH 042
U.S. Nuclear Regulatory
Commission
Washington, D.C. 20555

Mrs. Elizabeth Apfelberg
c/o Nancy Culver
192 Luneta Drive
San Luis Obispo, CA 93401

Mr. Frederick Eissler
Scenic Shoreline Preservation
Conference, Inc.
4623 More Mesa Drive

Sandra A. Silver
1760 Alisal Street
San Luis Obispo, CA 93401

Malcolm H. Furbush, Esq.
Vice President and
General Counsel
Philip A. Crane, Esq.
Douglas A. Oglesby
Pacific Gas & Electric Company
31st Floor
77 Beale Street, Room 3127
San Francisco, CA 94106

Gordon Silver
1760 Alisal Street
San Luis Obispo, CA 93401

Joel Reynolds
John Phillips, Esq.
Center For Law In-
The Public Interest
10203 Santa Monica Boulevard
Fifth Floor
Los Angeles, CA 90067

Bruce Norton, Esq.
3216 N. Third Street
Suite 202
Phoenix, Arizona 85012

Janice E. Kerr, Esq.
Lawrence Q. Garcia, Esq.
California Public Utilities
Commission
5346 State Building
350 McAllister Street
San Francisco, California 94102

Arthur C. Gehr, Esq.
Snell & Wilmer
3100 Valley Center
Phoenix, Arizona 85073

David S. Fleischaker, Esq.